Spring 1977

DIRECT MEASUREMENTS OF EXCITED-STATE LIFETIMES IN GROUP-II AND GROUP-III ATOMS

MARK DOUGLAS HAVEY

INFORMATION TO USERS

This material was produced from a microfilm copy of the original document. While the most advanced technological means to photograph and reproduce this document have been used, the quality is heavily dependent upon the quality of the original submitted.

The following explanation of techniques is provided to help you understand markings or patterns which may appear on this reproduction.

1. The sign or "target" for pages apparently lacking from the document photographed is "Missing Page(s)". If it was possible to obtain the missing page(s) or section, they are spliced into the film along with adjacent pages. This may have necessitated cutting thru an image and duplicating adjacent pages to insure you complete continuity.

2. When an image on the film is obliterated with a large round black mark, it is an indication that the photographer suspected that the copy may have moved during exposure and thus cause a blurred image. You will find a good image of the page in the adjacent frame.

3. When a map, drawing or chart, etc., was part of the material being photographed the photographer followed a definite method in "sectioning" the material. It is customary to begin photoing at the upper left hand corner of a large sheet and to continue photoing from left to right in equal sections with a small overlap. If necessary, sectioning is continued again — beginning below the first row and continuing on until complete.

4. The majority of users indicate that the textual content is of greatest value, however, a somewhat higher quality reproduction could be made from "photographs" if essential to the understanding of the dissertation. Silver prints of "photographs" may be ordered at additional charge by writing the Order Department, giving the catalog number, title, author and specific pages you wish reproduced.

5. PLEASE NOTE: Some pages may have indistinct print. Filmed as received.

University Microfilms International
300 North Zeeb Road
Ann Arbor, Michigan 48106 USA
St. John's Road, Tyler's Green
High Wycombe, Bucks, England HP10 8HR

DIRECT MEASUREMENTS OF EXCITED-STATE LIFETIMES IN GROUP II AND GROUP III ATOMS

by

MARK D. HAVEY

B.S., University of Maine, 1973

A DISSERTATION

Submitted to the University of New Hampshire

In Partial Fulfillment of

The Requirements for the Degree of

Doctor of Philosophy

Graduate School

Department of Physics

May, 1977

This thesis has been examined and approved.

L. C. Balling

Thesis director, L.C. Balling, Professor of Physics

Robert E. Houston

Robert E. Houston, Jr., Professor of Physics

John E. Mulhern Jr.

John E. Mulhern, Jr., Professor of Physics

Harvey K. Shepard

Harvey K. Shepard, Assoc. Professor of Physics

John J. Wright

John J. Wright, Assoc. Professor of Physics

Date

ACKNOWLEDGEMENTS

I would like to express gratitude to my advisor, Dr. L.C. Balling, for his encouragement and support throughout this work. I also wish to thank Dr. J.J. Wright for his assistance during the early stages of the experiments, and Dr. H.K. Shepard, Dr. R.E. Houston and Dr. J.E. Mulhern for their critical reading of this thesis.

Finally, I would like to thank my wife, Keitha, for her unfailing patience, understanding and encouragement throughout all of my graduate work.

This work was supported by the National Science Foundation and the Research Corporation.

TABLE OF CONTENTS

PAGE

LIST OF TABLES vi

LIST OF FIGURES. vii

ABSTRACT ix

I. INTRODUCTION 1

II. THEORY 4

2.1 ELECTRIC DIPOLE TRANSITIONS 4

2.2 FLUORESCENCE SIGNALS. 8

2.3 THERMAL MIXING OF THE SR ^{3}P MULTIPLET 11

III. APPARATUS. 22

3.1 INTRODUCTION. 22

3.2 APPARATUS FOR SHORT-LIFETIME MEASUREMENTS . . 22

3.2.1 Lasers 22

3.2.2 Photomultiplier Tube 27

3.2.3 Oscilloscope and Camera. 31

3.2.4 Sample Cell. 32

3.3 APPARATUS FOR LONG-LIFETIME MEASUREMENTS. . . 36

3.3.1 Lasers 36

3.3.2 Detection Electronics. 36

3.3.3 Sample Cell. 37

IV. EXPERIMENT AND RESULTS 41

4.1 INTRODUCTION. 41

4.2 SHORT-LIFETIME MEASUREMENTS 41

4.3 SYSTEMATIC ERRORS 49

PAGE

4.4 RESULTS AND DISCUSSION (SHORT LIFETIMES) 64

4.5 SR $^3P_1$ STATE MEASUREMENTS. 68

4.6 $^3P_1$ STATE-SYSTEMATIC EFFECTS 76

4.7 RESULTS ($^3P_1$ STATE). 87

4.8 CONCLUSION 88

REFERENCES 90

BIBLIOGRAPHY 95

APPENDIX I 96

APPENDIX II. 100

APPENDIX III 103

LIST OF TABLES

NUMBER PAGE

1. SR ^3P FINE-STRUCTURE LEVELS 14
2. LASER DYES (3500 Å - 7500 Å). 30
3. COLLISIONALLY MIXED CA SINGLET LEVELS 63
4. LIFETIMES OF THE $^3S_1$ STATES IN MG, CA AND SR. . . . 65
5. LIFETIMES OF VARIOUS STATES IN THE SINGLET SERIES OF CA. 66
6. LIFETIME OF THE LOWEST $^2S_{1/2}$ STATE OF AL, GA, IN AND TL. 67
7. SUMMARY OF RECENT THEORETICAL AND EXPERIMENTAL VALUES FOR THE SR $^3P_1$ LIFETIME 88
8. COEFFICIENTS OF THE OBSERVED SIGNAL, S(t) 102

LIST OF FIGURES

NUMBER		PAGE
1.	SR TRIPLET SERIES	10
2.	CALCULATED AND EXPERIMENTAL SIGNALS FOR SR $^3S_1$ STATE FLUORESCENCE	13
3.	THERMAL EQUILIBRIUM POPULATIONS IN THE SR ^3P MULTIPLET	18
4.	SR $^3P_1$ STATE LIFETIME CORRECTION FACTOR	21
5.	APPARATUS USED IN MEASUREMENTS REQUIRING TWO-STEP EXCITATION	24
6.	APPARATUS USED IN MEASUREMENTS REQUIRING ONE-STEP EXCITATION	26
7.	SCHEMATIC N_2 LASER-PUMPED DYE LASER	29
8.	SAMPLE CELL USED IN THE SHORT-LIFETIME MEASUREMENTS	34
9.	SAMPLE CELL USED IN THE LONG-LIFETIME MEASUREMENTS.	39
10.	LOW LYING, TRIPLET SERIES ENERGY LEVELS OF CA, MG, AND SR.	44
11.	ENERGY LEVELS OF THE CA SINGLET SERIES.	46
12.	LOW LYING ENERGY LEVELS OF THE GROUP III ATOMS.	48
13.	DATA FROM A GA $^2S_{1/2} \rightarrow {}^2P_{3/2}$ FLUORESCENCE SIGNAL.	51
14.	MG $^3S_1$ STATE LIFETIME VS. BUFFER GAS PRESSURE	57
15.	CA $4s6s\,^1S_0$ STATE LIFETIME VS. HE GAS PRESSURE	60
16.	CA $4s6s\,^1S_0$ STATE LIFETIME VS. KR GAS PRESSURE	62
17.	HISTOGRAM OF THE TL $^2S_{1/2}$ STATE LIFETIME DATA	70
18.	HISTOGRAM OF THE MG $^3S_1$ STATE LIFETIME DATA	72
19.	DATA FROM A SR $^3P_1$ STATE FLUORESCENCE SIGNAL.	75
20.	SR $^3P_1$ STATE LIFETIME VS. HE PRESSURE	78
21.	SR $^3P_1$ STATE SHORT DECAY TIME VS. KR GAS PRESSURE	82

NUMBER PAGE

22. SR $^3P_1$ STATE LONG DECAY TIME VS. KR AND XE GAS PRESSURE 84

23. SR $^3P_1$ STATE LONG DECAY TIME VS. TEMPERATURE 86

24. RATES FOR MIXING IN (a.) NEARBY CA LEVELS AND (b.) SR ^3P LEVELS 98

ABSTRACT

The lifetimes of a large number of excited states in the Group II and Group III atoms have been measured. Among these states are the $5s5p\,^3P_1$ metastable state of Sr and the lowest $^3S_1$ state of Mg, Ca, and Sr. Also measured were the lifetimes of the lowest $^2S_{1/2}$ states of Al, Ga, In and Tl, and the lifetimes of several $^1S_0$ and $^1D_2$ states of Ca. The excited states were populated by one- and two-step dye laser excitation, and the lifetimes determined by direct observation of the subsequent resonance or branching fluorescence. The results obtained for states in the triplet series of the Group II atoms are: $\tau(Sr\ ^3P_1) = (21.0 \pm 1.0)\mu sec$, $\tau(Mg\ ^3S_1) = (9.7 \pm 0.5)$ nsec, $\tau(Ca\ ^3S_1) = (11.7 \pm 0.6)$ nsec, $\tau(Sr\ ^3S_1) = (12.9 \pm 0.7)$ nsec.

CHAPTER I

INTRODUCTION

The recent accessibility of short-pulse,tunable dye-lasers and fast oscilloscopes has allowed the direct determination of lifetimes of highly excited states in atoms and ions. The precision of these experiments is comparable to that obtained in level-crossing experiments, which usually give the best results for lifetimes of states connected directly to the ground state.

Lifetime values that are convertible to oscillator strengths have important astrophysical applications[1], being useful for determinations of the relative abundances of elements in stellar atmospheres. Even when branching precludes the conversion of a lifetime value into an oscillator strength, the measured lifetime can be used to check oscillator strength calculations, since the reciprocal of the lifetime is proportional to the sum of the oscillator strengths for transitions out of the level under study.

A number of workers have made use of the short pulses produced by N_2-pumped dye-lasers to perform a variety of experiments, including lifetime measurements, on highly excited states in the alkali atoms[2-4] and in iron.[5] In these experiments the excited state of interest was selectively populated by pulsed laser radiation, and the subsequent resonance or branching fluorescence monitored to determine the lifetime of the state.

In this thesis, experiments performed to measure a large number of excited-state lifetimes in the Group II and Group III atoms are described, and the results of these experiments presented. Among the states whose lifetime was measured are the lowest $^3S_1$ state of Ca, Mg, and Sr; the lowest $^2S_{1/2}$ state of Al, Ga, In, and Tl; and several doubly excited S and D states in the singlet series of Ca. Also included are results from experiments measuring the lifetime of the $^3P_1$ metastable state of Sr and the rate of collisional redistribution, by various inert gases, of population within the ^3P multiplet of Sr.

In all of these experiments, the excited levels were populated by one- or two-step dye-laser excitation and the lifetime determined by simply observing the decay of the fluorescence emitted from the excited states. All of the states studied, except the Sr $^3P_1$ metastable state, decay by electric dipole transitions to lower levels, and thus have lifetimes on the order of 10 nsec. The Sr $^3P_1$ state decays by a spin-forbidden ($\Delta S = 1$) electric dipole transition to the Sr $^1S_0$ ground state, and has a lifetime of about 21 μsec.

The direct method of measuring lifetimes used here has certain advantages over other techniques used to determine oscillator strengths and lifetimes of highly excited states. In particular, the measurements are not complicated by repopulation of the excited state by radiative cascade, as is the case with some beam-foil and electron bombardment experiments. Also, results obtained from emission and

anomalous dispersion experiments have a strong dependence on the metal vapor density, which is not usually the case for the direct methods. Results from anomalous dispersion, or hook method, measurements often suffer the added disadvantage of having to be normalized to independently determined lifetime data.

The principal disadvantage of the direct method, as used here, is the effect that the finite response time of the electronic detection system could have on the measured lifetimes. The measurements on the 4.7 nsec lifetime Ca $^1P_1 \leftrightarrow {}^1S_0$ principal line yielded the shortest lifetime value determined here. Evidently, to directly determine lifetimes from signals this short requires a detection system with a response time fast compared to 4.7 nsec. As will be discussed in detail later in this thesis, the detection electronics used in these experiments did reasonably satisfy this criterion, having a response time in the 1.2 - 1.5 nsec range.

Before proceeding to a detailed description of the experiments and to the results of the experiments, the theoretical ideas behind the measurements will be discussed. In particular, the theory of electric dipole and spin-forbidden electric dipole transitions will be outlined, and a theoretical expression for the fluorescence signal expected in the experiments will be derived. As the observed Sr $^3P_1$ state lifetime depends on the relative populations of the various ^3P fine structure levels (in thermal equilibrium), expressions for these quantities will also be obtained.

CHAPTER II

THEORY

2.1 ELECTRIC DIPOLE TRANSITIONS

Most of the states whose lifetime was measured decay by electric dipole (ED) transitions to lower lying energy levels. These transitions, which have rates on the order of 10^8/sec, produce the most intense optical lines observed in atomic spectra. The spontaneous decay rate, in the electric dipole approximation, from a state $|\gamma_o\rangle$ to a lower state $|\gamma_k\rangle$ is given by [6]

$$R_K = \frac{4}{3}\alpha\frac{\omega_K^3}{c^2}|\langle\gamma_K|\vec{R}|\gamma_o\rangle|^2. \qquad (1)$$

Here α is the fine structure constant, ω_k is the resonant frequency of the $|\gamma_o\rangle \rightarrow |\gamma_k\rangle$ transition, and $e\vec{R}$ is the total electric dipole moment of the atom. This expression for R_k includes the contributions from both polarizations of the emitted light and is the total rate integrated over all propagation directions of the emitted radiation.

Since, for the most part, we are considering optical transitions in light atoms, a suitable representation for $|\gamma_o\rangle$ and $|\gamma_k\rangle$ is $|\Gamma LSJM\rangle$, where Γ labels the electronic configuration of the valence electrons. In this representation, the rate R_k vanishes unless certain conditions on the changes in J, M, L, and S during the transition are made. These

selection rules are that $\Delta J = (0, \pm 1)$, $\Delta L = (0, \pm 1)$, $\Delta M = (0, \pm 1)$, and $\Delta S = 0$. A further requirement (independent of representation) is that, as $\vec{R}$ is an odd operator, the wave function parity must change in the transition.

Now, if $|\gamma_o>$ decays to a number of lower levels $|\gamma_k>$ $(k = 1, N)$, as is usually the case, the R_k must be summed over all lower levels. The total observed rate is thus

$$R = \frac{4}{3}\alpha \sum_{K=1}^{N} \frac{\omega_K^3}{c^2} \left| \langle \gamma_K | \vec{R} | \gamma_o \rangle \right|^2 . \tag{2}$$

The lifetime of the state $|\gamma_o>$ is the mean time an electron spends in that state, given by

$$\tau = \frac{\int_0^\infty t\, e^{-Rt}\, dt}{\int_0^\infty e^{-Rt}\, dt} = \frac{1}{R} . \tag{3}$$

Thus the lifetime of a state is the reciprocal of the total rate out of that state.

The contribution, R_k, to R in the above expression vanishes unless $S_k = S_o$ $(\Delta S = 0)$. This means that, in this approximation, R itself is zero if $\Delta S = 1$ and $|\gamma_o>$ decays to only one lower level. However, these intercombination transitions, where $\Delta S = 1$, are observed in the spectrum of many atoms. For example, the $^3P_1 \rightarrow {}^1S_0$ transitions are observed with moderate rates (10^2 - 10^4/sec) in the alkaline earth atoms.

These spin forbidden transitions occur because the $|\Gamma JMLS\rangle$ states are not strictly eigenstates of the total atomic Hamiltonian. In particular, the spin-orbit interaction Hamiltonian is not diagonal (for atoms with more than one electron) in this set of states. As L and S separately do not commute with $H_{s.o.}$, they are no longer good quantum numbers, although (as $H_{s.o.}$ is small) they are still approximately good quantum numbers. What breaks down is our characterization of the electron wavefunctions by precise values of L and S. What one needs to obtain an expression for the (spin-forbidden) transition rate is the first correction to the $|\Gamma JMLS\rangle$ states. This correction is calculated by stationary state perturbation theory, and is given by

$$|\Psi_K\rangle = \sum_{K \neq i} |\gamma_i\rangle \frac{\langle \gamma_i | H_{s.o.} | \gamma_K \rangle}{E_i - E_K} \quad . \tag{4}$$

Here $H_{s.o.}$ is the spin-orbit interaction Hamiltonian and E_k the energy of the k^{th} unperturbed eigenstate. $H_{s.o.}$ includes the spin-own-orbit, spin-other-orbits, and spin-spin interaction terms, expressions for which can be found in Mizushima[8]. The sum extends over all bound and continuum states of the unperturbed Hamiltonian, but usually only a few terms contribute significantly[9] to $|\Psi_k\rangle$.

The mixing of $|\Gamma JMLS\rangle$ states by $H_{s.o.}$ is illustrated by the calculations of Nussbaumer[10] on the $2s2p^3P_1 \rightarrow 2s^2\,{}^1S_0$ intercombination transition in CIII. He shows that only five $|\Gamma JMLS\rangle$ states contribute significantly to the expansions of

the new $^1S_0$ and $^3P_1$ wavefunctions. The expansion of $\Psi(^1S_0)$ contains contributions from several ^3P states of the unperturbed Hamiltonian (H_o), while the expansion of $\Psi(^3P_1)$ contains significant contributions from ^1P terms of H_o. Because of this mixing of singlet and triplet terms, the matrix elements of the dipole operator will be nonzero between the new wavefunctions, yielding a nonzero decay rate for the $^1S_0 \leftrightarrow {}^3P_1$ transition.

The spin-orbit mixing is thus sufficient to account for observations of intercombination lines in the Group II atoms (which have the same outer shell structure as CIII). A number of workers[11-13] have used this approach to obtain alkaline earth $^3P_1 \rightarrow {}^1S_0$ transition rates which are in moderate agreement with experimental values. However, Luc-Koenig[11] has shown that, in the case of Sr, other relativistic effects must be taken into account to yield good agreement with experimental values for the $^3P_1$ state lifetimes.

2.2 FLUORESCENCE SIGNALS

If the time dependence of the resonant laser light populating a multilevel system is known, the time behavior of the various levels of the system can be derived. In this section an expression for the fluorescence signal arising from the Sr $^3S_1 \rightarrow {}^3P_{2,1,0}$ transitions is derived, and the result compared to an actual fluorescence signal obtained in the course of the lifetime measurements.

The relevant Sr energy levels are shown in Figure 1. The resonant laser was tuned to the $^3P_1 \rightarrow {}^3S_1$ transition wavelength, and the branching fluorescence corresponding to the $^3S_1 \rightarrow {}^3P_2$ transition detected to obtain the fluorescence signal. By observing the branching fluorescence, complications due to scattered laser light in comparing the calculated signal to the observed signal were avoided.

The time dependence of the laser pulse, L(t), determined experimentally to be nearly triangular with a base of about ten nsec, was

$$L(t) = \begin{cases} \frac{I_0}{5}t & 0 \le t < 5 \\ \frac{I_0}{5}(10-t) & 5 \le t < 10 \\ 0 & t \ge 10 \,. \end{cases} \qquad (5)$$

Here $I_0/5$ is a constant related to the beam intensity. The time, t, is in nsec. Using this expression for L(t), the rate equations for the populations of the $^3S_1$ state are

$$\frac{dN}{dt} = -\Gamma N + \frac{I_0}{5} n t \qquad 0 \le t < 5,$$

$$\frac{dN}{dt} = -\Gamma N + \frac{I_0}{5} n (10-t) \qquad 5 \le t < 10, \qquad (6)$$

$$\frac{dN}{dt} = -\Gamma N \qquad t > 10.$$

In these equations Γ is the natural decay rate of the $^3S_1$ level and n is the population of the metastable $^3P_1$ state. Note that the equations are only approximate in that

FIGURE 1

SR TRIPLET SERIES

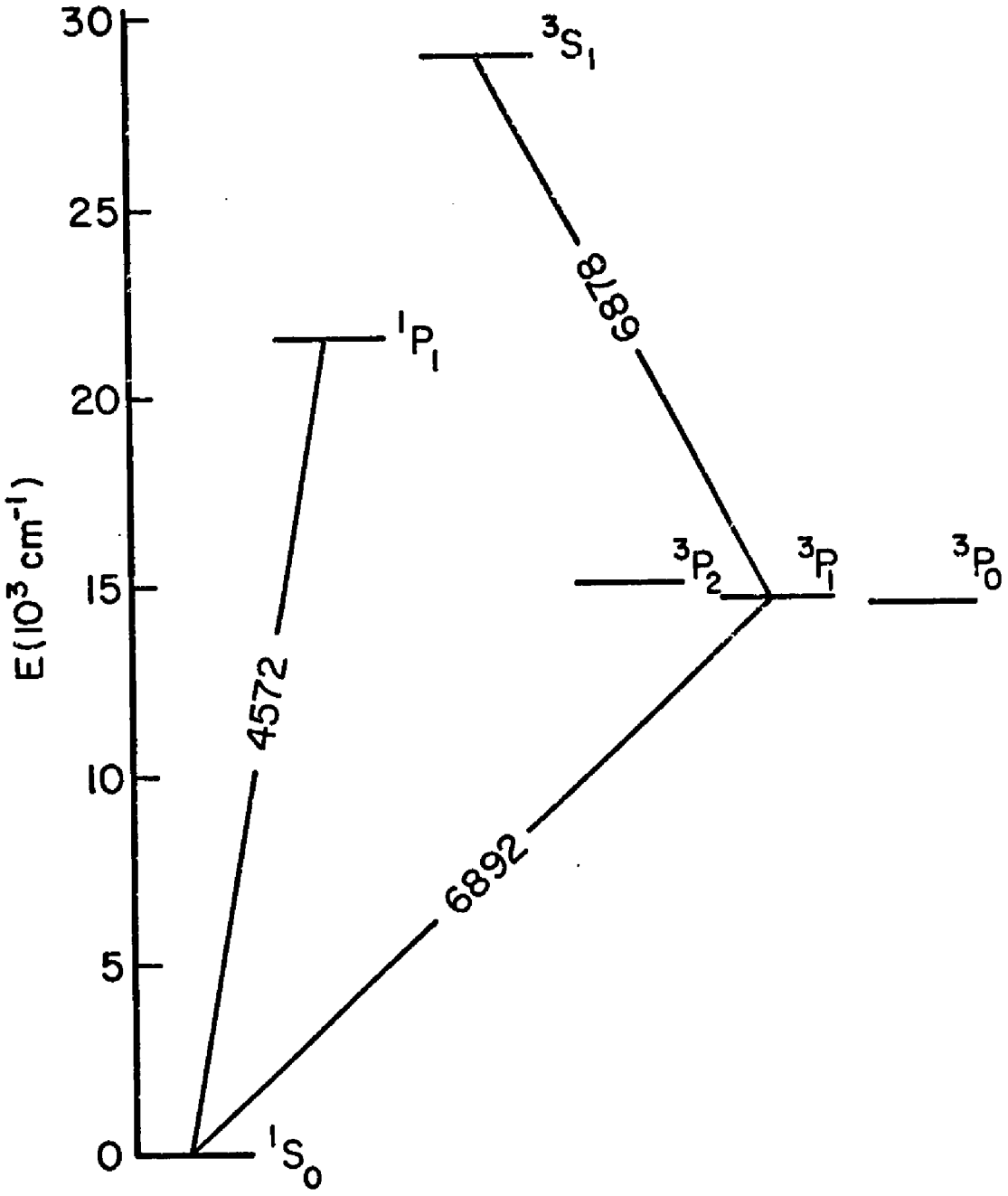
30
25
20
15
10
5
0
E(10³ cm⁻¹)
³S₁
¹P₁
³P₂
³P₁
³P₀
¹S₀
6878
4572
6892

stimulated emission and depopulation of the $^3P_1$ state have been ignored. The principal motivation for these approximations is that most of the signals observed were linear in the laser power, implying that processes non-linear in I_o are small. With the initial condition that N(0) = 0, the solution to these equations is

$$N(t) = \frac{I_o n}{5\Gamma^2} \begin{cases} e^{-\Gamma t} + \Gamma t - 1 & 0 \le t < 5 \\ (1 - 2e^{5\Gamma})\, e^{-\Gamma t} - \Gamma t + (1 + 10\Gamma) & \\ (1 - 2e^{5\Gamma} + e^{10\Gamma})\, e^{-\Gamma t} & t > 10 \end{cases} \quad (7)$$

Figure 2 shows how the calculated expression for N(t), drawn as the solid curve, compares with the actual fluorescence signal arising from the $^3S_1 \rightarrow {}^3P_2$ transition in Sr. A least squares fit to the data points (open circles) for $t \geq 10$ nsec with $I_o n/\Gamma^2$ and Γ as parameters yielded 134.4 and 0.081/nsec for these quantities. The excellent agreement obtained over the entire range of the signal justifies the assumptions made in the model and shows that the entire fluorescence signal observed is reasonably well understood.

2.3 THERMAL MIXING OF THE SR ^3P MULTIPLET

The ^3P metastable state of Sr has three fine structure components corresponding to the different values of |J| (2,1,0) allowed for this L = 1, S = 1 level. Furthermore, as seen in Table 1, these fine structure levels are separated in energy by considerably less than the average thermal energy, 3/2 kT.

FIGURE 2

CALCULATED AND EXPERIMENTAL SIGNALS FOR

SR $^3S_1$ STATE FLUORESCENCE

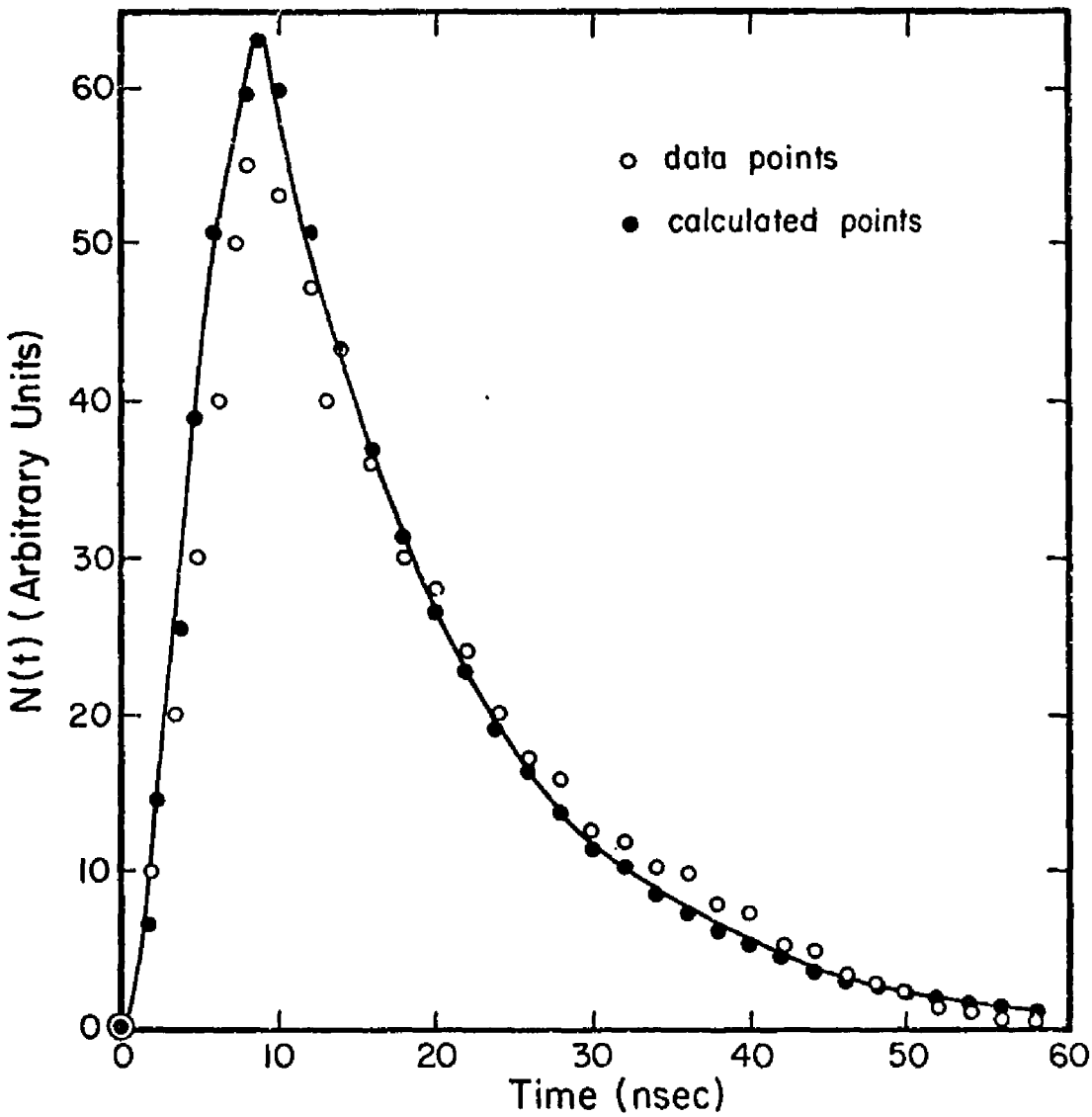
o data points
● calculated points
N(t) (Arbitrary Units)
Time (nsec)
0
10
20
30
40
50
60

TABLE 1

SR ^3P FINE-STRUCTURE LEVELS

ΔE_{21}	ΔE_{20}	ΔE_{10}	3/2 kT (@ 720°K)
394.2	581.0	186.8	752.8

In the experiments involving the Sr ^3P levels, various inert buffer gases were used to inhibit diffusion of the metastable atoms out of the interaction region. The buffer gas atoms, having thermal energies larger than the fine structure separations of the $^3P_{2,1,0}$ levels, mixed the ^3P levels by inelastic collisions with excited Sr atoms. In this section an expression will be derived for the expected $^3P_1 \rightarrow {}^1S_0$ fluorescence signal for the case where the collision rate is so high that the populations of the ^3P levels are in thermal equilibrium. An approximation to the case where the rate is sufficiently low that the mixing rate into, and out of, the $^3P_1$ level is linear in the buffer gas density is presented in Appendix III.

When the mixing rate between the various ^3P fine structure components is very fast compared to the rate that the $^3P_1$ level decays to the ground state, the levels will be driven into thermal equilibrium. This means that the relative population of the various levels will depend only on the degeneracies (g_k) of the levels and on the Boltzmann factor, $e^{-\Delta E/kT}$.

In particular, if n_0, n_1 and n_2 are the populations of the $^3P_0$, $^3P_1$ and $^3P_2$ levels and if the energy separations of the levels are

$$\Delta E_{21} = E(^3P_2) - E(^3P_1), \tag{8}$$

$$\Delta E_{10} = E(^3P_1) - E(^3P_0), \tag{9}$$

then

$$\frac{n_2}{n_1} = \frac{g_2}{g_1} e^{-\Delta E_{21}/KT} \tag{10}$$

and

$$\frac{n_0}{n_1} = \frac{g_0}{g_1} e^{-\Delta E_{01}/KT} . \tag{11}$$

If we define N_0 to be the total population of the ^3P state, then the relative populations are

$$\frac{n_0}{N_0} = \frac{\frac{g_0}{g_1} e^{-\Delta E_{01}/KT}}{1 + \frac{g_0}{g_1} e^{-\Delta E_{01}/KT} + \frac{g_2}{g_1} e^{-\Delta E_{21}/KT}} , \tag{12}$$

$$\frac{n_1}{N_0} = \frac{1}{1 + \frac{g_0}{g_1} e^{-\Delta E_{01}/KT} + \frac{g_2}{g_1} e^{-\Delta E_{21}/KT}} , \tag{13}$$

$$\frac{n_2}{N_0} = \frac{\frac{g_2}{g_1} e^{-\Delta E_{21}/KT}}{1 + \frac{g_0}{g_1} e^{-\Delta E_{01}/KT} + \frac{g_2}{g_1} e^{-\Delta E_{21}/KT}} . \tag{14}$$

These expressions for the relative populations are plotted vs. temperature in Figure 3.

Now, the ^3P system can decay by the spin forbidden $^3P_2 \rightarrow {}^1S_0$ and $^3P_1 \rightarrow {}^1S_0$ transitions to the Sr $^1S_0$ ground state, the $^3P_0 \rightarrow {}^1S_0$ transition being strictly forbidden. However, as the electric quadrupole ($\Delta J = 2$) $^3P_2 \rightarrow {}^1S_0$ transition decays with a rate about 10^{-6} times that of the electric dipole $^3P_1 \rightarrow {}^1S_0$ transition[13], the ^3P system will decay primarily via the $^3P_1 \rightarrow {}^1S_0$ transition. The rate equation for $N_o(t)$ is thus

$$\frac{dN_o}{dt} = -\gamma_1 n_1$$

$$= \frac{-\gamma_1 N_0}{1 + \frac{g_0}{g_1} e^{-\Delta E_{01}/KT} + \frac{g_2}{g_1} e^{-\Delta E_{21}/KT}} \quad . \tag{15}$$

With the condition that $N_o(0) = N$, the solution to this equation is

$$N_o(t) = N e^{-\frac{\gamma_1 t}{\beta(T)}} \quad , \tag{16}$$

where

$$\beta(T) = 1 + \frac{g_0}{g_1} e^{-\Delta E_{01}/KT} + \frac{g_2}{g_1} e^{-\Delta E_{21}/KT} \quad . \tag{17}$$

The temperature dependent factor $\beta(T)$, which makes the observed

FIGURE 3

THERMAL EQUILIBRIUM POPULATIONS

IN THE SR ^{3}P MULTIPLET

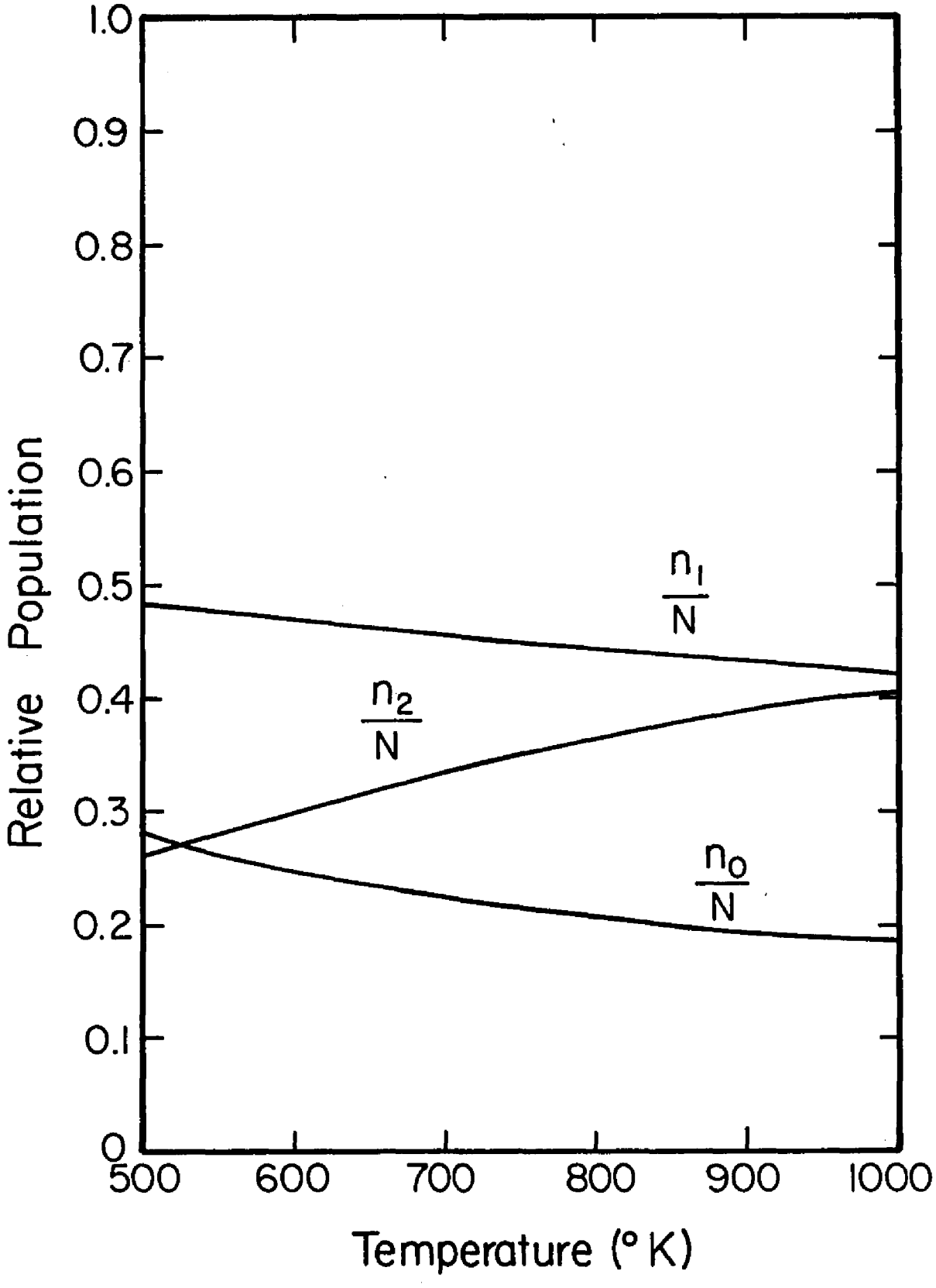
1.0
0.9
0.8
0.7
0.6
0.5
0.4
0.3
0.2
0.1
0
Relative Population
$\frac{n_1}{N}$
$\frac{n_2}{N}$
$\frac{n_0}{N}$
500
600
700
800
900
1000
Temperature (° K)

lifetime β/γ_1, longer than the natural lifetime $1/\gamma_1$, is plotted vs. temperature in Figure 4. This lengthening of the natural lifetime was taken into account in analyzing the results of the lifetime measurements on the Sr $^3P_1$ state.

FIGURE 4

SR $^3P_1$ STATE LIFETIME CORRECTION FACTOR

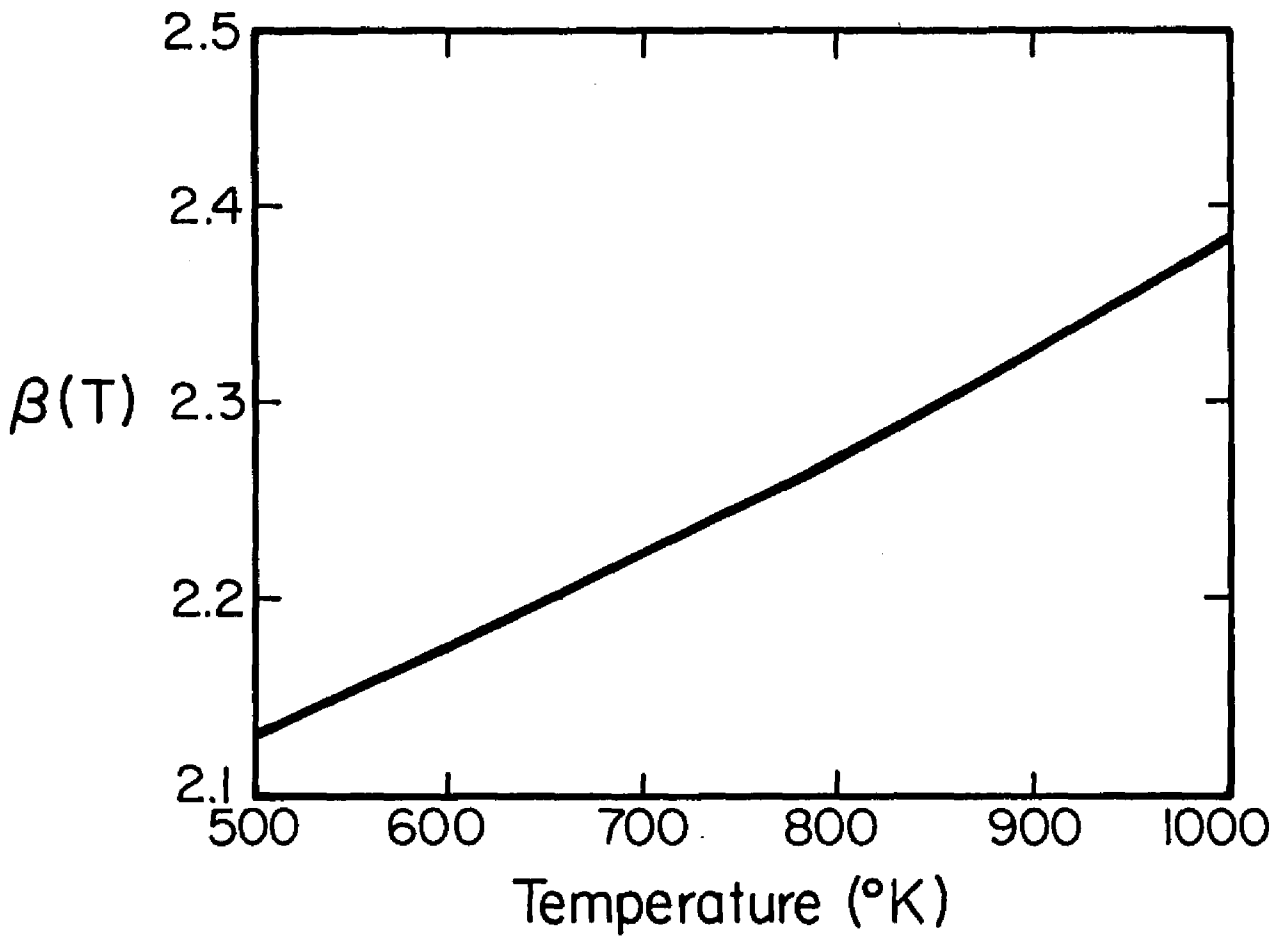
2.5
2.4
β(T) 2.3
2.2
2.1
500
600
700
800
900
1000
Temperature (°K)

CHAPTER III

APPARATUS

3.1 INTRODUCTION

Because of the great disparity in decay rates between electric-dipole and spin-forbidden electric dipole transitions, different experimental set-ups were used for each of the groups of measurements. The fast ($\sim 10^8$/sec) decay rate of ED transitions requires short excitation pulses and fast detection electronics, while the small ($\sim 10^4$/sec) decay rate typical of spin-forbidden transitions requires more powerful light sources and higher signal detection efficiency. Figure 5 shows schematically the experimental apparatus used for the short-lifetime measurements requiring two-step excitation. The apparatus used for lifetime measurements requiring only one-step excitation is schematically shown in Figure 6. This figure applies to both the long-lived and the short-lived state measurements, although the specific instruments used in each of these cases were different.

3.2 APPARATUS FOR SHORT-LIFETIME MEASUREMENTS

3.2.1 Lasers

An AVCO C950-B, N_2-laser provided the 10 mJ, 10 nsec pumping radiation for the dye lasers used in these experiments. When step-wise excitation was required, the mirror of the

FIGURE 5

APPARATUS USED IN LIFETIME MEASUREMENTS

REQUIRING TWO-STEP EXCITATION

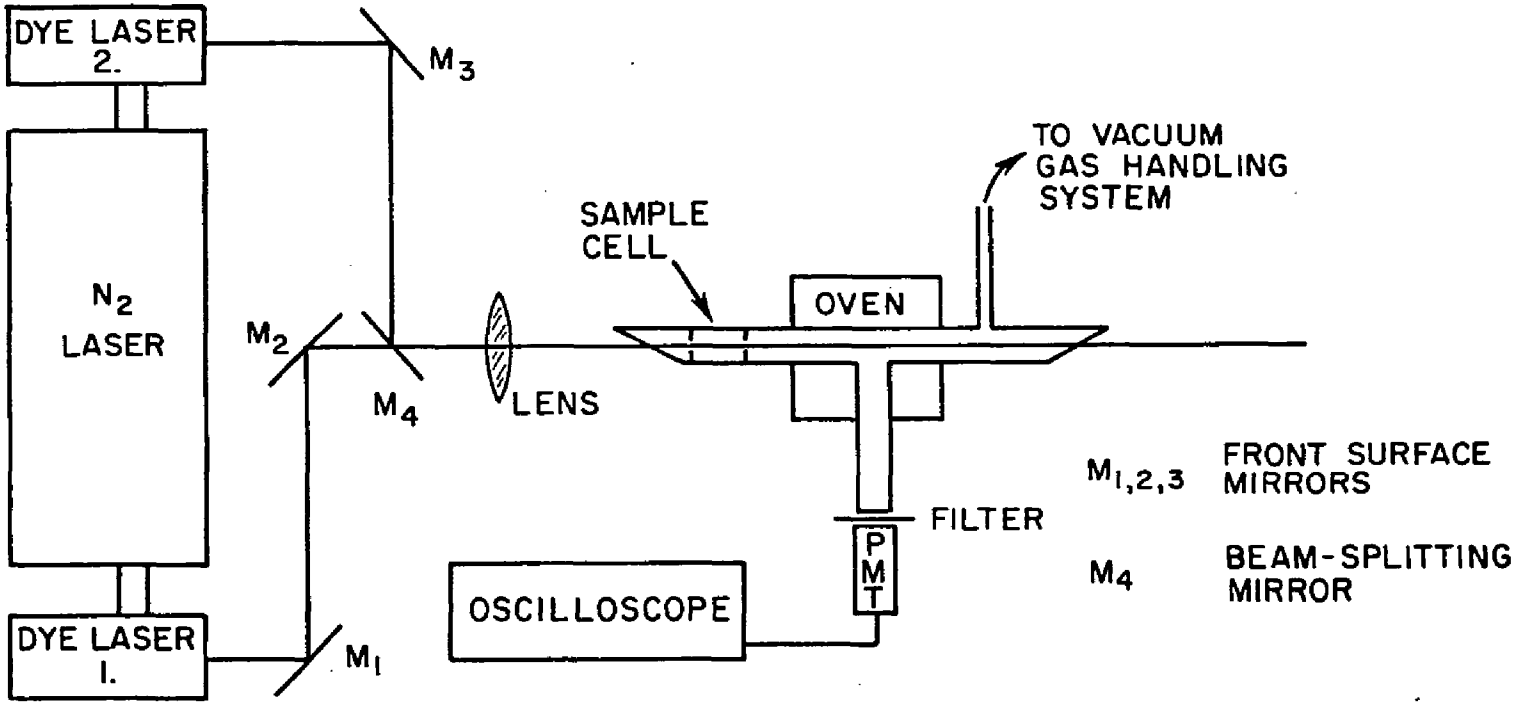
DYE LASER 2.
M_3
N_2 LASER
M_2
M_4
LENS
SAMPLE CELL
TO VACUUM GAS HANDLING SYSTEM
OVEN
FILTER
PMT
OSCILLOSCOPE
DYE LASER 1.
M_1
$M_{1,2,3}$ FRONT SURFACE MIRRORS
M_4 BEAM-SPLITTING MIRROR

FIGURE 6

APPARATUS USED IN LIFETIME MEASUREMENTS

REQUIRING ONE-STEP EXCITATION

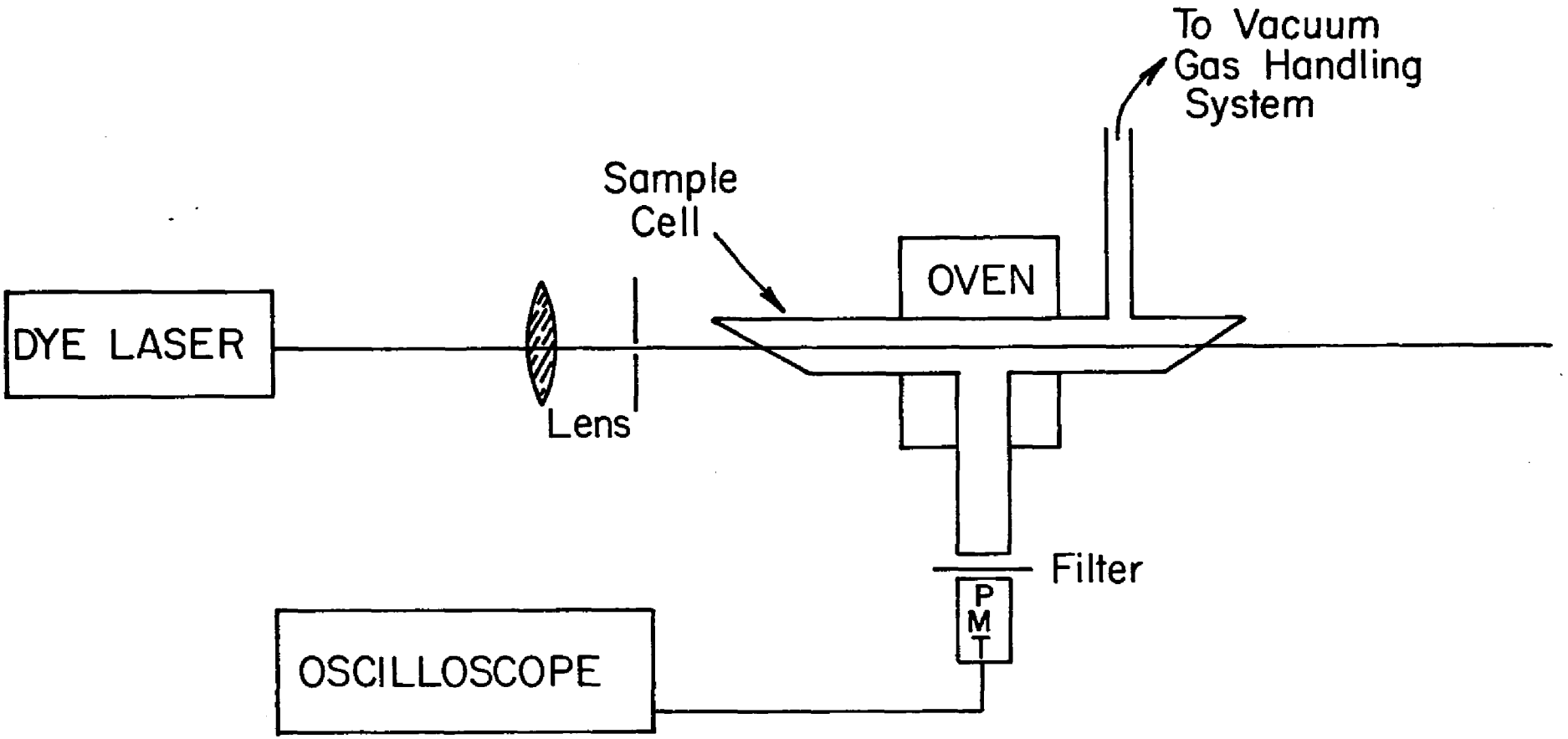
To Vacuum
Gas Handling
System
Sample
Cell
OVEN
DYE LASER
Lens
Filter
P
M
T
OSCILLOSCOPE

N_2-laser was removed to permit the simultaneous pumping of two dye-lasers. Otherwise, the mirror was left on in order to provide more pumping light intensity for the one dye laser. To produce collinear laser beams for the two-step excitations, several broad band mirrors and a beam-splitting mirror were used, as shown in Figure 5. The collinear beams were focused into the interaction region by a long-focal length lens.

Each dye laser consisted of a static dye cell, a beam expander, diffraction grating, and an output mirror. No precise measurements of laser bandwidth or output power were made, but the bandwidth of the lasers was estimated to be 1 Å and the 4-10 nsec dye laser pulses had estimated typical energies of 10 mJ in the interaction region. Because a diffraction grating was used to set the laser wavelength, the output beam of each dye-laser was linearly polarized. A schematic diagram of a dye-laser as used in these experiments is shown in Figure 7.

A variety of laser dyes was used to provide optical dye laser radiation in the 3500 Å - 7500 Å range. The relevant information on these dyes[14-15] is summarized in Table 2.

3.2.2 Photomultiplier Tube

The fluorescence signals were detected by an RCA 8645 photomultiplier tube, which has an S-20 cathode and a nominal rise time of 1.2 nsec. These two characteristics of the tube made it nearly ideal for detecting visible and near visible

FIGURE 7

SCHEMATIC N_2-LASER PUMPED DYE LASER

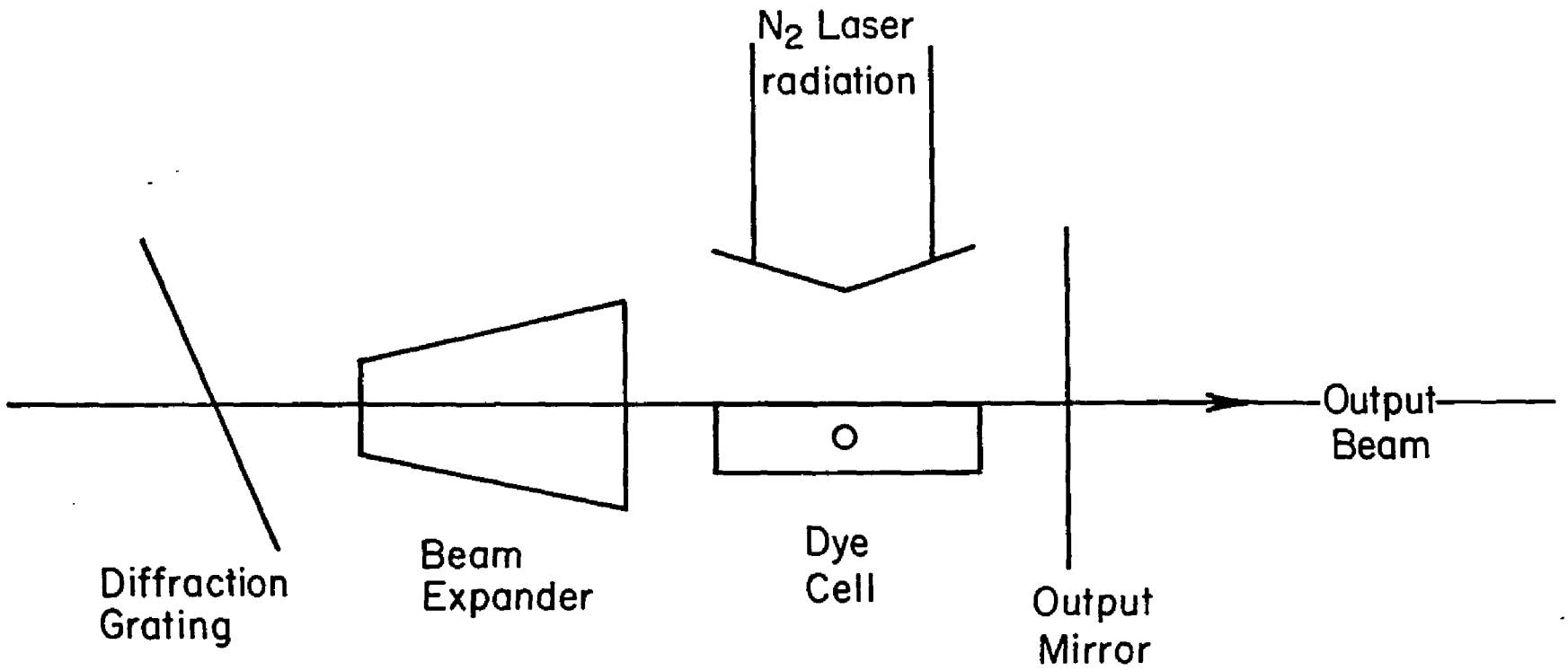
N_2 Laser
radiation
Output
Beam
Diffraction
Grating
Beam
Expander
Dye
Cell
Output
Mirror

TABLE 2

LASER DYES (3500 Å - 7500 Å)

LASER DYE	WAVELENTH	SOLVENT
PBD	3600 - 3900	toluene
POPOP-bis	4120 - 4300	toluene
7-Diethylamino-4-methylcoumarin	4400 - 4900	ethanol
Rhodamine 6G	5650 - 6250	ethanol
Rhodamine B	5900 - 6500	ethanol
Oxazine-1-perchlorate + Rhodamine 6G	7050 - 7500	ethanol
Cresyl Violet perchlorate + Rhodamine B	6500 - 6910	ethanol
4-Methyl-unbelliferone	4100 - 5500	slightly acidic (HCl) ethanol

fluorescence signals with short decay times. The PMT output impedence was about 55Ω[16], well matched to the 50Ω input impedence of the amplifier of the oscilloscope used to display the signals. Power was supplied to the PMT by a Harrison 6515A DC power supply operated at about 1800 V. All of the electronic detection equipment was well shielded from electrical noise.

The fluorescence signal of interest was selected by narrow-band interference filters[17] placed in front of the PMT. These 50 Å bandwidth filters eliminated unwanted cascading fluorescence and prevented saturation of the PMT by glow from the hot oven or by stray light. Occasionally a ¼-meter Ebert spectrometer was used in place of interference filters to selectively observe the cascading or direct fluorescence spectrum. The spectrometer had a bandwidth of about 10 Å.

3.2.3 Oscilloscope and Camera

The PMT output signals were displayed and photographically recorded on a Tektronix 7903 oscilloscope, the amplifier of which had a 500 MHz bandwidth and a 50Ω input impedence. A coaxial lead, which was short to minimize possible RC stretching of the signals, connected the PMT output to the amplifier. The oscilloscope's time base was calibrated with a General Radio 1164A frequency synthesizer.

A Tektronix C-51 camera was used to record the oscilloscope trace of the fluorescence decay signals. The camera was equipped with an electronic shutter, an f/1.2 lens system

with a magnification of 0.5, and an adjustable aperture. To avoid difficulties in timing the signal to the opening of the camera shutter, the oscilloscope was swept and the electronic shutter opened synchronously by an external trigger pulse generated by the N_2-laser power supply. This trigger pulse was delayed 20 - 25 nsec by an AD-YU Type 801C variable delay line to properly time the oscilloscope sweep with the PMT output signal.

Because of the short decay time of the transient signals, photographs were taken with the very fast Type 410 Polarscope Land roll film[18], which has an ASA rating of 10,000. It was found that film with a lower ASA rating (Polaroid Type 47, 3000 ASA) did not respond to the trace sufficiently fast to record the signal.

3.2.4 Sample Cell

The quartz sample cells used to contain the metal vapor were specially designed to minimize scattering of laser radiation into the PMT. As shown in Figure 8, the entrance and exit windows were cut at Brewster's angle. This minimized scattering of the linearly polarized laser light from the window surfaces. Two brass stops located just inside the front window further reduced the level of scattered laser light reaching the PMT. Even so, some laser light scattered by imperfections in the quartz or Pyrex windows was light-piped to the PMT. The effect that this might have had on the lifetime measurements is discussed in Chapter IV.

FIGURE 8

SAMPLE CELL USED IN THE SHORT-LIFETIME MEASUREMENTS

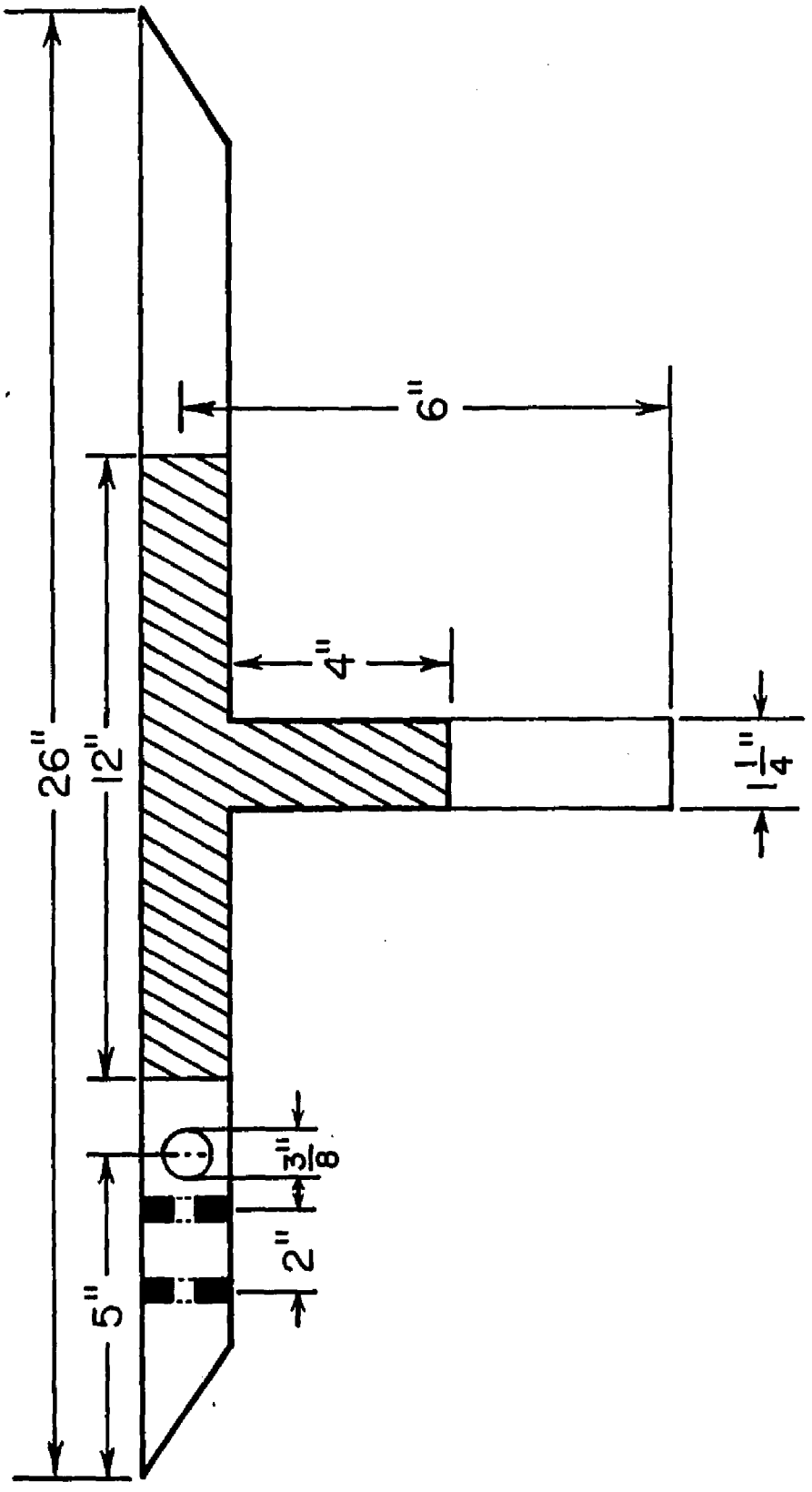
6"
4"
26"
12"
1 1/4"
3/8"
2"
5"

A diagram of the fluorescence sample cell with relevant dimensions is presented in Figure 8. The cell was a quartz fluorescence cell lined with tantalum foil.[20] The Ta foil liner prevented reaction of the metal vapor with the hot quartz walls. Windows were of Pyrex or of quartz and were attached to the cell by Torr Seal, a low vapor-pressure epoxy.

The interaction region of the cell was surrounded by a well-insulated firebrick oven, as indicated in Figure 5. The oven contained a small heater coil carrying typically 10A (AC), which was capable of heating the oven to above 1000°C. The temperature was monitored by a Platinum-Rhodium thermocouple in conjunction with a 151 R Keithley null detector and a HP 5245L electronic counter. One junction of the thermocouple was in direct contact with the cell while the other, located outside the oven, was at room temperature (∿22°C).

Prior to being baked out, each cell was rinsed with benzene and then acetone. This removed any oil that might have been on the inner surface of the cell. Each cell was then washed out with a 10% HF solution and distilled water to remove any additional material which might have been trapped in the cell.

Each cell was connected to an oil-free, vacuum-gas handling system and was baked out at 900 - 950°C until the background pressure was in the 10^{-7} - 10^{-6} Torr range. The cell was then cooled and opened to air, metal[21] was introduced, and the cell was reconnected to the vacuum system. To prevent metal vapor from condensing on the cell windows, a buffer gas was admitted to the cell. The cell was then heated to 850 -

900°C, well above the melting point of the Group III metals and Sr. As Ca and Mg melt above 1000°C, these metals could not be melted. It was found that the strong heating of the metal, which drives off gas trapped inside the metal, greatly reduced the background pressure in the cells. For these experiments done in evacuated cells, the background pressure during runs was in the 10^{-4} - 10^{-5} Torr range.

3.3 APPARATUS FOR LONG-LIFETIME MEASUREMENTS

3.3.1 Lasers

The $^3P_1$ or metastable state was populated by radiation from a Phase-R DL-22 flashlamp-pumped dye laser. The 1 μsec, 0.1 J pulses produced by this laser had an estimated bandwidth of 0.5 Å and a power density of about 2 MW/cm^2 in the interaction region. High power densities were necessary because of the small absorption rate out of the ground state to the $^3P_1$ state.

A 5×10^{-5} molar solution of Cresyl Violet Perchlorate and ethanol was used in the dye laser to produce laser radiation at the 6893 $^1S_0 \rightarrow {}^3P_1$ transition wavelength. The dye laser output wavelength was determined with a ½-meter, Jarrell-Ash spectrophotometer, which had been calibrated with an electrodeless, r.f. Sr lamp.

3.3.2 Detection Electronics

An RCA 7102 photomultiplier (S-1 cathode), in conjunction with a narrowband interference filter centered at 6893 Å,

was used to detect the $^3P_1 \rightarrow {}^1S_0$ resonance fluorescence. The 50 Å bandwidth filter prevented saturation of the PMT by glow from the hot oven and eliminated stray light. As shown in Figure 6, two optical stops and a long focal length lens were used to create a spatially well-defined laser beam, thus minimizing scattering of laser radiation into the PMT. Power was supplied to the tube by a Harrison 6515A DC power supply operated at 1500 V.

The PMT output was displayed and recorded on a Tektronix 549 storage oscilloscope, which had an input impedence of about 1 kΩ. The time base was calibrated with a General Radio 1164-A frequency synthesizer. The long-lived phosphor and fine-lined graticule of this oscilloscope allowed a signal to be stored and accurately recorded directly from the oscilloscope screen. Lifetimes deduced from data taken in this manner were reproducible (from signal to signal) to better than 10%.

3.3.3 Sample Cell

A schematic diagram of the sample cell, with relevant dimensions, is shown in Figure 9. The cell was a quartz fluorescence cell lined with Ta foil, which prevented reaction of the Sr metal vapor with the hot quartz walls. The windows were quartz, and were blown onto the cell after it had been lined with Ta. The cell was chemically cleaned in the same manner as those used for short-lifetime measurements.

FIGURE 9

SAMPLE CELL USED IN THE LONG-LIFETIME MEASUREMENTS

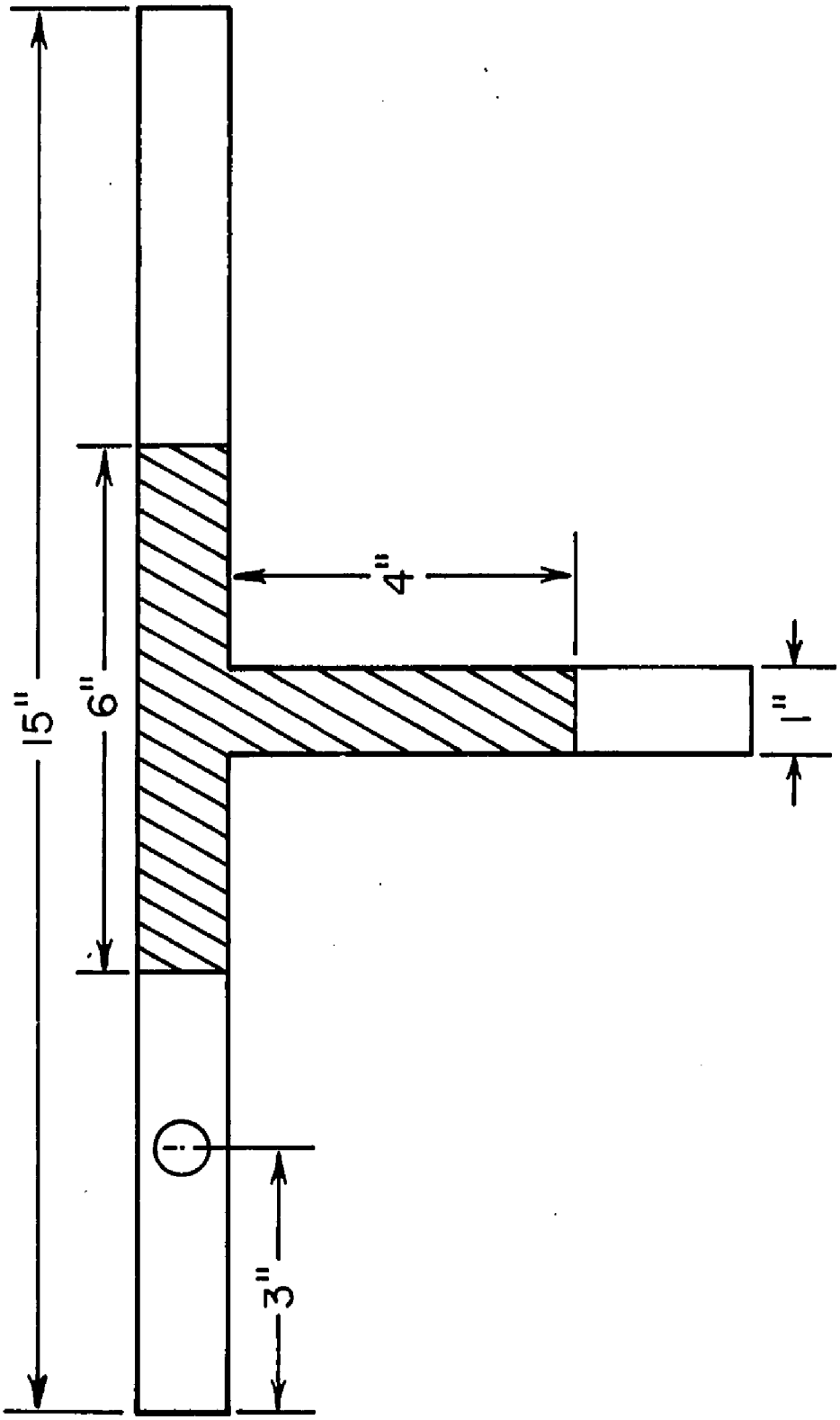
15"
6"
4"
1"
3"

The apparatus used to measure the temperature and the construction of the oven and heater are the same as described in Section 3.2.4.

The cell was connected to a vacuum-gas handling system and was baked out at 1000°C until the background pressure was $\sim 9 \times 10^{-8}$ Torr. The cell was then cooled and opened to air, Sr metal was introduced and the cell was reconnected to the vacuum system. A research grade[22] buffer gas (Ar) was introduced to prevent diffusion of Sr vapor to the cell windows and the cell was heated to ~900°C, well above the Sr melting point. The cell was then cooled and the contaminated gas pumped out. Background pressure was in the 10^{-7} Torr range.

CHAPTER IV

EXPERIMENT AND RESULTS

4.1 INTRODUCTION

The lifetime measurements described in this thesis were made by direct observation of the decay of the fluorescence emitted from laser-excited states. In this chapter I will describe how optimum fluorescence signals were obtained, and how data was acquired and analyzed. The results of the lifetime measurements, along with a discussion of the errors, will also be presented.

4.2 SHORT-LIFETIME MEASUREMENTS

The dye lasers were set to the appropriate transition wavelengths by monitoring the laser output with a ½-meter spectrophotometer. This was a sufficiently reliable method that fluorescence signals were usually obtained upon simply heating the oven until a suitable density of metal atoms was produced in the cell. For the one-step excitations, the laser was then tuned to resonance by maximizing the fluorescence from the excited state. For levels populated by step-wise excitation, the fluorescence from the lower, and then from the upper, excited state was maximized by tuning the appropriate dye laser. Further tuning of either dye-laser usually resulted in a decrease in fluorescence intensity from the upper level, indicating that the

excitation was doubly resonant. A photomultiplier tube-interference filter combination at right angles to the exciting laser beam directly viewed the fluorescence from the interaction region. For convenience, the Tektronix storage oscilloscope was used to display signals while the lasers were tuned to resonance. All lifetime data, however, was recorded with the fast oscilloscope.

The $^3S_1$ level of Ca, Mg, or Sr was populated by two-step excitation via the metastable $^3P_1$ level of that atom, while the excited S and D states in the Ca singlet series were populated by two-step excitation via the $4s4p\,^1P_1$ level. Populating the lowest $^2S_{1/2}$ state of Al, Ga, In, and Tl required only one-step excitation out of the $^2P_{1/2}$ atomic ground state. All these excitation paths, and the transitions by which fluorescence was observed are indicated in Figures 10-12.

After the laser wavelengths were set, the sample cell was heated to produce a density of metal atoms suitable for obtaining fluorescence signals. For the measurements on the principal line of the Group III atoms, a ground state atom density in the 10^{-7} - 10^{-6} Torr range produced excellent signals that were not radiation trapped. Measurements on the Ca $^1S_0$ and $^1D_2$ levels required ground state densities in the 10^{-4} - 10^{-3} Torr range, while those made in the Ca, Mg, or Sr triplet series required a density on the order of 1 Torr for Mg and 10^{-3} Torr for Sr and Ca. These higher metal atom densities were necessary because the $^3S_1$ level was populated via

FIGURE 10

LOW LYING, TRIPLET SERIES ENERGY

LEVELS OF CA, MG, AND SR

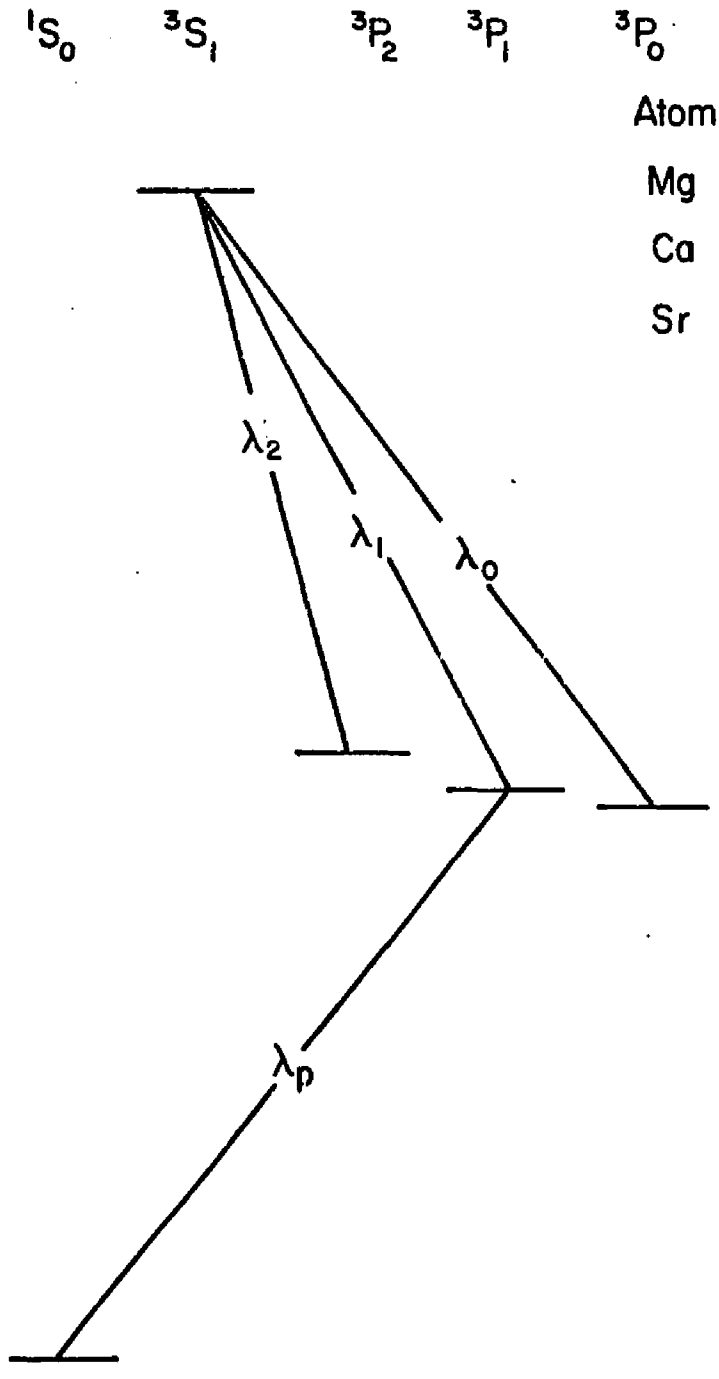

Atom	λ_p	λ_0	λ_1	λ_2
Mg	4572	5169	5174	5185
Ca	6573	6104	6122	6162
Sr	6892	6791	6878	7070

FIGURE 11

ENERGY LEVELS OF THE CA SINGLET SERIES

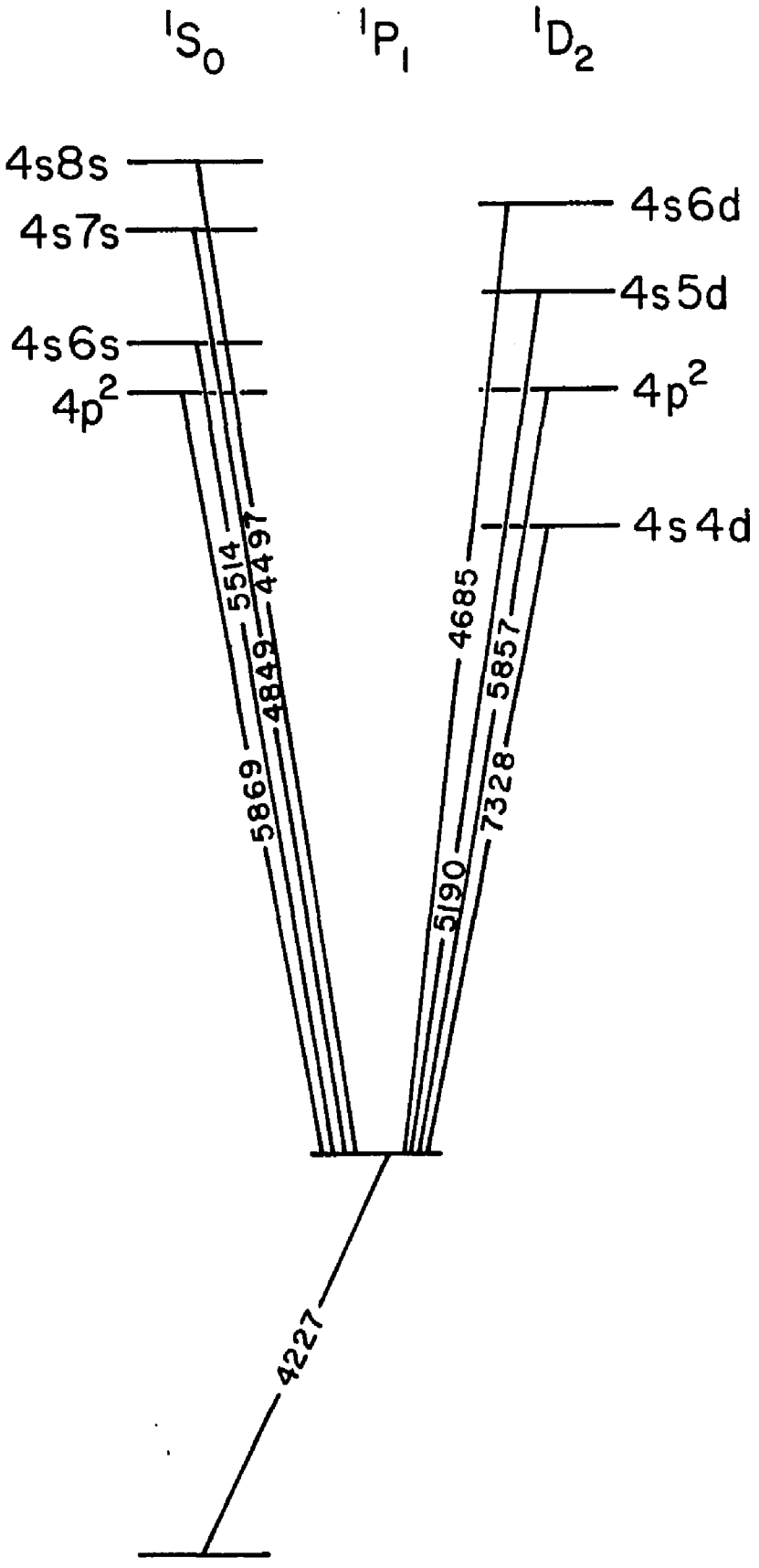
$^1S_0$
$^1P_1$
$^1D_2$
4s8s
4s7s
4s6s
$4p^2$
4s6d
4s5d
$4p^2$
4s4d
5514
4497
4849
5869
4685
5857
5190
7328
4227

FIGURE 12

LOW LYING ENERGY LEVELS OF

THE GROUP III ATOMS

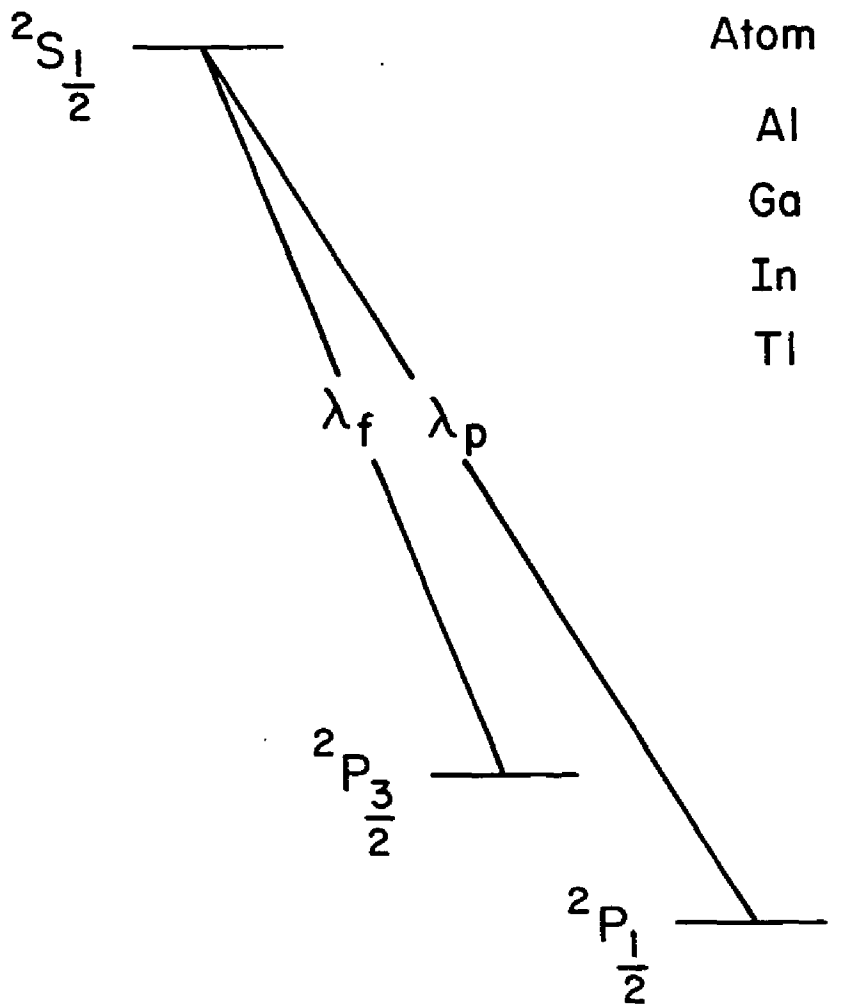

Atom	λp (A°)	λf (A°)
Al	3944.0	3961.5
Ga	4032.9	4172.1
In	4101.8	4511.3
Tl	3775.7	5350.5

the difficult-to-excite $^3P_1$ metastable state. Operating temperatures ranged from ∿320°C for measurements on the Ca $4s4p^1P_1$ state to ∿1000°C for those on the $3s^24s^2S_{1/2}$ state of Al.

Lifetime data was acquired from photographs of the oscilloscope trace of the exponential decay of the fluorescence emitted from the excited states. A result for each photograph was determined by plotting the signal amplitude semilogarithmically as a function of time out three lifetimes, starting at about t = 15 nsec. The portion of the signal used to obtain the plots is indicated in Figure 13, which is data from a typical Ga $^2S_{1/2} \rightarrow {}^2P_{3/2}$ fluorescence signal. An estimate of the slope of the straight line portion of this curve yielded each photograph's lifetime value.

For measurements of the lifetime of the $^3S_1$ state of Mg, Ca, and Sr, and of the $^2S_{1/2}$ state of Al, Ga, In, and Tl, 45 - 60 such photographs were taken in a final data run. All other lifetime values were obtained from a final data run of typically 25 photographs. The final data run was carried out only after checks for a number of possible systematic effects on the lifetime were made. The checks for systematic errors are discussed in detail in the next section.

4.3 SYSTEMATIC ERRORS

There are a number of possible sources of systematic error to be considered in the measurements. Collisional quenching and mixing of the levels under study, radiation

FIGURE 13

DATA FROM A GA $^2S_{\frac{1}{2}} - {}^2P_{\frac{3}{2}}$ FLUORESCENCE SIGNAL

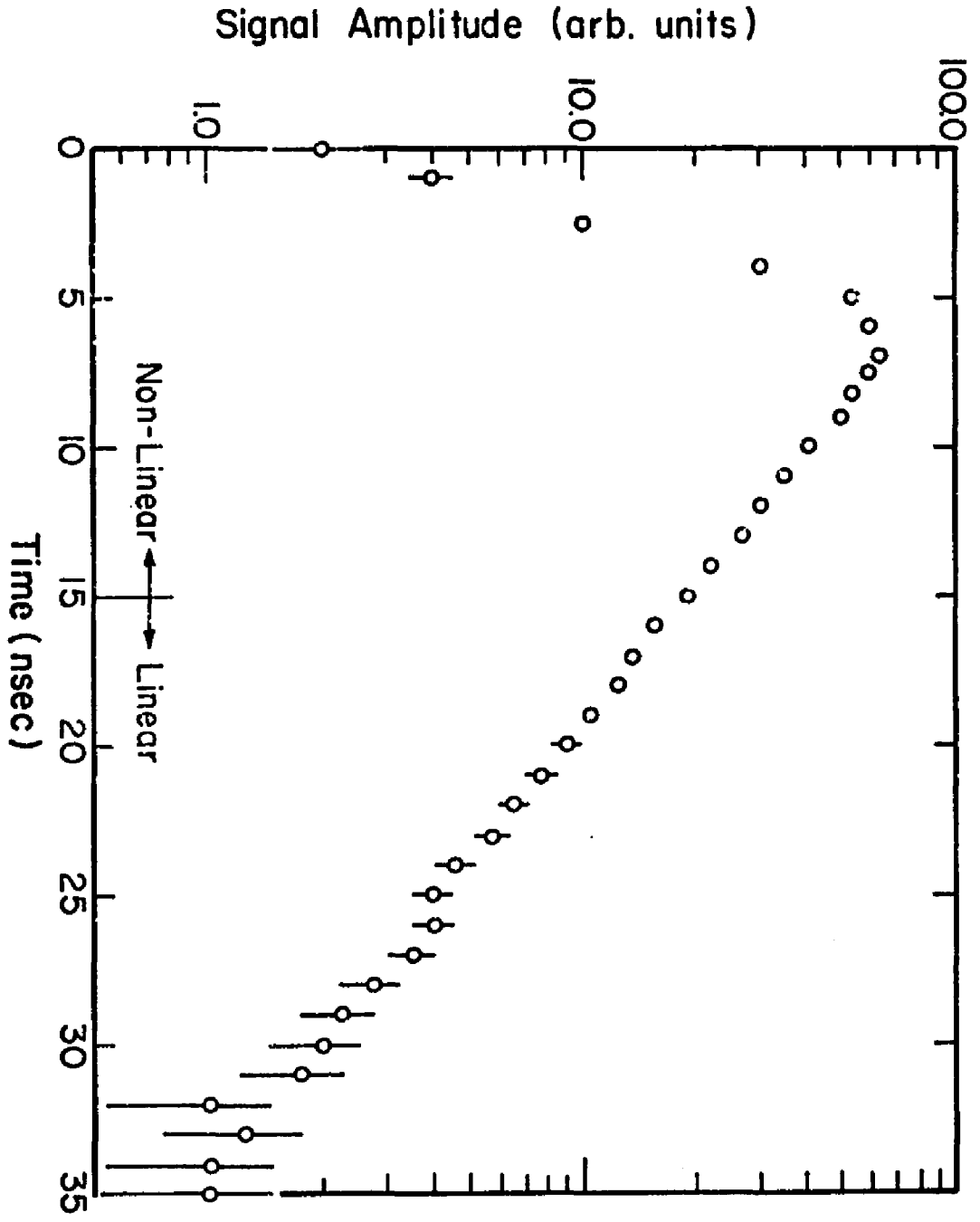
Signal Amplitude (arb. units)
1.0
10.0
100.0
0
5
10
15
20
25
30
35
Time (nsec)
Non-Linear
Linear

trapping and stimulated emission are all possible sources of systematic error. Signal distortion due to photomultiplier saturation, nonlinearities in the PMT response, and signal distortion due to an insufficiently fast PMT-oscilloscope response time are possible important sources of instrument-induced error which much be considered.

Except for in the Ca $4s4p\,^1P_1$ state lifetime measurements, no lengthening of the short lifetimes by radiation trapping was observed. By decreasing the metal vapor density until no change in the $^1P_1$ lifetime was observed, radiation trapping was eliminated as a source of systematic error in this measurement. The Ca vapor density could be varied over a factor of two with no change in the observed lifetime.

For the Al measurements, the metal vapor density could be increased an order of magnitude above the density at which we were just able to measure lifetimes with no increase in the observed lifetime. For the Ga, In, and Tl experiments the density could be increased a factor of thirty with no observable increase in the lifetime. It is because the $^2S_{1/2}$ branches to both the $^2P_{3/2}$ and $^2P_{1/2}$ states that the Group III $^2S_{1/2}$ state lifetimes are not more sensitive to radiation trapping. Since the $^2P_{3/2}$ state, being far above the ground state, is virtually unpopulated at t = 0, repopulation of the $^2S_{1/2}$ state, and hence radiation trapping, can only take place out of the $^2P_{1/2}$ state.

For the measurements of the Ca $^1S_0$ and $^1D_2$ state lifetimes, and for the Mg, Ca, and Sr $^3S_1$ state lifetime

measurements, the metal vapor density was varied over typically an order of magnitude with no change in the observed lifetime. This was expected, as the intermediate states ($^1P_1$ or $^3P_1$) were only weakly populated relative to the ground state and, in the case of the $^1P_1$ Ca level, decayed rapidly to the $^1S_0$ ground state.

For each of the measurements, checks were made to see if the observed lifetime depended on the intensity of the laser populating the upper state. Using neutral density filters, the laser intensity was varied over an order of magnitude with no change in the observed lifetime. No change in the lifetime was observed by varying the intensity of the laser populating the intermediate state over an order of magnitude. For the two-step excitation measurements, this served as an added check on the effect of radiation trapping as, in this case, the degree of radiation trapping depends on the intermediate state density.

At the highest laser powers, evidence was seen of infrared Dicke superradiance[23-26] from some of the $^1S_0$ and $^1D_2$ Ca levels to nearby $^1P_1$ and $^1F_3$ levels, resulting in a rapid depopulation of the excited state. Using the ¼-meter spectrometer, the accompanying buildup of the $^1P_1$ or $^1F_3$ level population was observed by tuning to the fluorescence signal from that state. The buildup exhibited a time delay which increased with decreasing laser power, and an amplitude which increased as the square of the laser intensity. These two effects are characteristic of Dicke superradiance[23,26].

The superradiant depopulation of the state being studied did not interfere with the lifetime measurement, because the lifetime was measured using the exponential tail of the fluorescence signal.

Collisional quenching of the excited states by impurity atoms or molecules can shorten the observed lifetime. As the amount of impurities driven from the cell walls increases roughly exponentially with cell temperature, it was expected that any quenching present would become very noticable as the temperature was increased. However, no shortening of the lifetime with increasing temperature was observed for any of the measurements, indicating that quenching by impurities was not a problem in these experiments. In the measurements on the Ca $^1P_1$ state, there was a possibility of quenching to the $^1S_0$ ground state by Ca-Ca collisions. The cross-section for this process, as measured by Penkin and Shabanova[27], is anomalously large, being about 2.9×10^{-12} cm^2. However, no quenching of the $^1P_1$ level was observed.

Because the measurements of the lowest $^2S_{1/2}$ state lifetime in the Group III atoms required low metal vapor densities, these measurements could be made in evacuated cells. Besides eliminating the perturbative effect that the presence of a buffer gas might have on the lifetime measurements, this allowed independent monitoring of the background pressure in the cells while runs were being made. Background pressures at operating temperatures were in the 10^{-6} - 10^{-5} Torr range, well below pressures at which significant impurity quenching of the excited state would take place.

In some of the lifetime measurements, an inert buffer gas (He, Kr, Xe) was used to inhibit diffusion of metal vapor atoms to the cell windows. For the measurements of the $^3S_1$ state lifetime of Mg, Ca, and Sr, the presence of the inert gas was found to have no observable effect on the lifetime. For the Mg $^3S_1$ measurements, He (8 - 75 Torr) and Xe (0.5 - 196 Torr) buffer gases were used, while for the Ca and Sr $^3S_1$ state lifetime measurements, Kr buffer gas was used. The Kr pressure in these experiments was varied from 1 to 12 Torr for Ca and from 1 to 99 Torr for Sr with no significant change in the observed lifetimes. The results for the Mg buffer gas pressure runs are presented in Figure 14, where each data point represents the arithmetic average of the results from 4 - 5 photographs.

In the measurements in the Ca singlet series, evidence was seen for collisional mixing of some of the $^1S_0$ and $^1D_2$ levels with neighboring excited states. This mixing is caused by inelastic collisions between inert gas atoms and excited Ca atoms, and for lower mixing gas pressures usually results in a lengthening of the observed lifetime (See Appendix I).

For each of these lifetime measurements, a ¼-meter spectrometer was used to scan, throughout the visible spectrum, for fluorescence from states populated by collisions with Kr buffer gas atoms. The states from which collisional mixing fluorescence was observed are presented in Table 3, along with the energy separation[12] of these states and the

FIGURE 14

MG $^3S_1$ STATE LIFETIME VS. BUFFER GAS PRESSURE

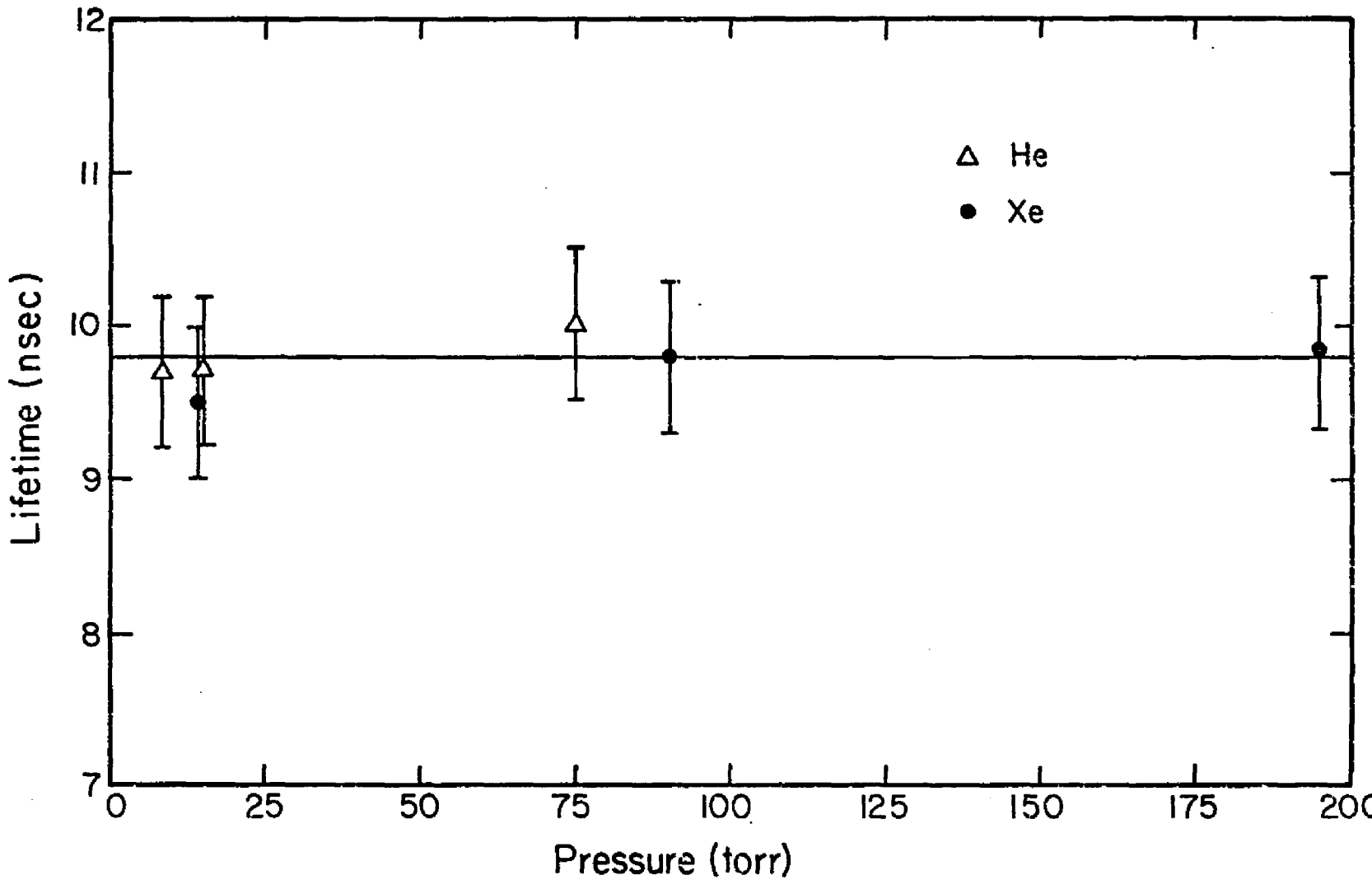
12
11
10
9
8
7
Lifetime (nsec)
0
25
50
75
100
125
150
175
200
Pressure (torr)
He
Xe

level whose lifetime was being measured. Those energy separations were invariably less than the average thermal energy ($\sim$775 cm^{-1}) of the colliding partners. During the diagnostic stage of the measurements, the Kr pressure was varied in the range 0.05 - 13 Torr. To eliminate the mixing as a source of error, the final data run for each of the Ca $^1S_0$ and $^1D_2$ states was always taken in an evacuated cell. The background pressure during the vacuum run was in the 10^{-6} - 10^{-5} Torr range.

The Ca $4s6s\,^1S_0$ state lifetime measurement typifies the effects that inert gas-Ca atom inelastic collisions had on the lifetime measurements. From Table 3 it is seen that the $^1S_0$ state mixes primarily with the $4s5d\,^1D_2$ and $4s4f\,^1F_3^0$ levels. Since the D and F states have M-degeneracies of 5 and 7, compared to 1 for the $^1S_0$ state, the S level can potentially mix to a large number of final states. The helium and krypton buffer gas pressure dependence of the $^1S_0$ lifetime is presented in Figures 15 and 16. The strong He pressure dependence indicates that He gas is a good mixer. From Figure 7, it is seen that the observed $^1S_0$ lifetime as a function of Kr gas pressure asymptotically approaches the "vacuum" value of 12.6 nsec. In fact, for P < 2.0 Torr Kr, no change in τ was observed, within the statistics of the measurements. This lack of mixing was borne out by the fact that no collisional fluorescence was seen in the ¼-meter scans at these low Kr gas pressures.

FIGURE 15

CA $4s6s\,^1S_0$ STATE LIFETIME VS. HE GAS PRESSURE

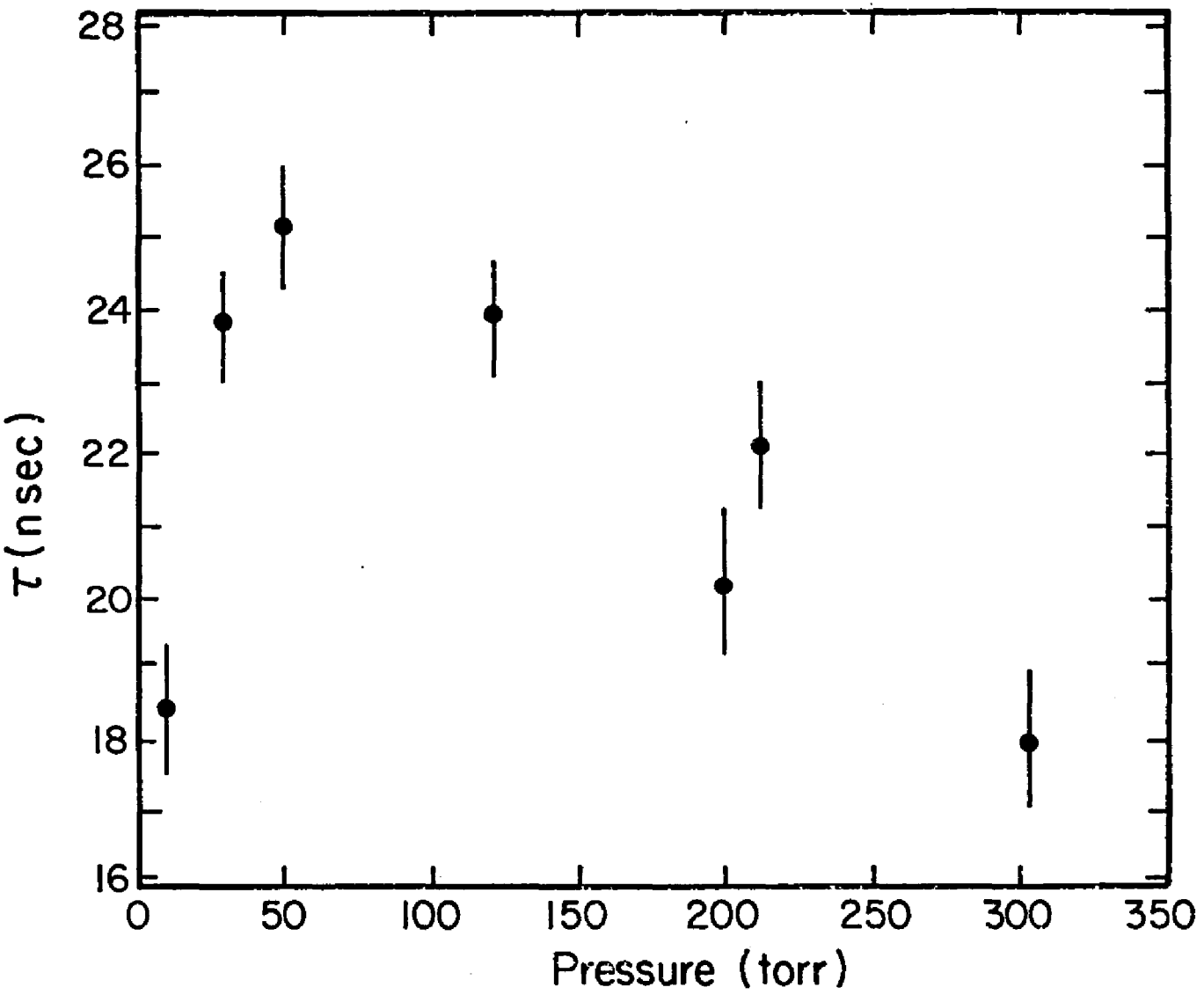
28
26
24
22
20
18
16
τ (n sec)
0
50
100
150
200
250
300
350
Pressure (torr)

FIGURE 16

CA $4s6s\,^1S_0$ STATE LIFETIME VS. KR GAS PRESSURES

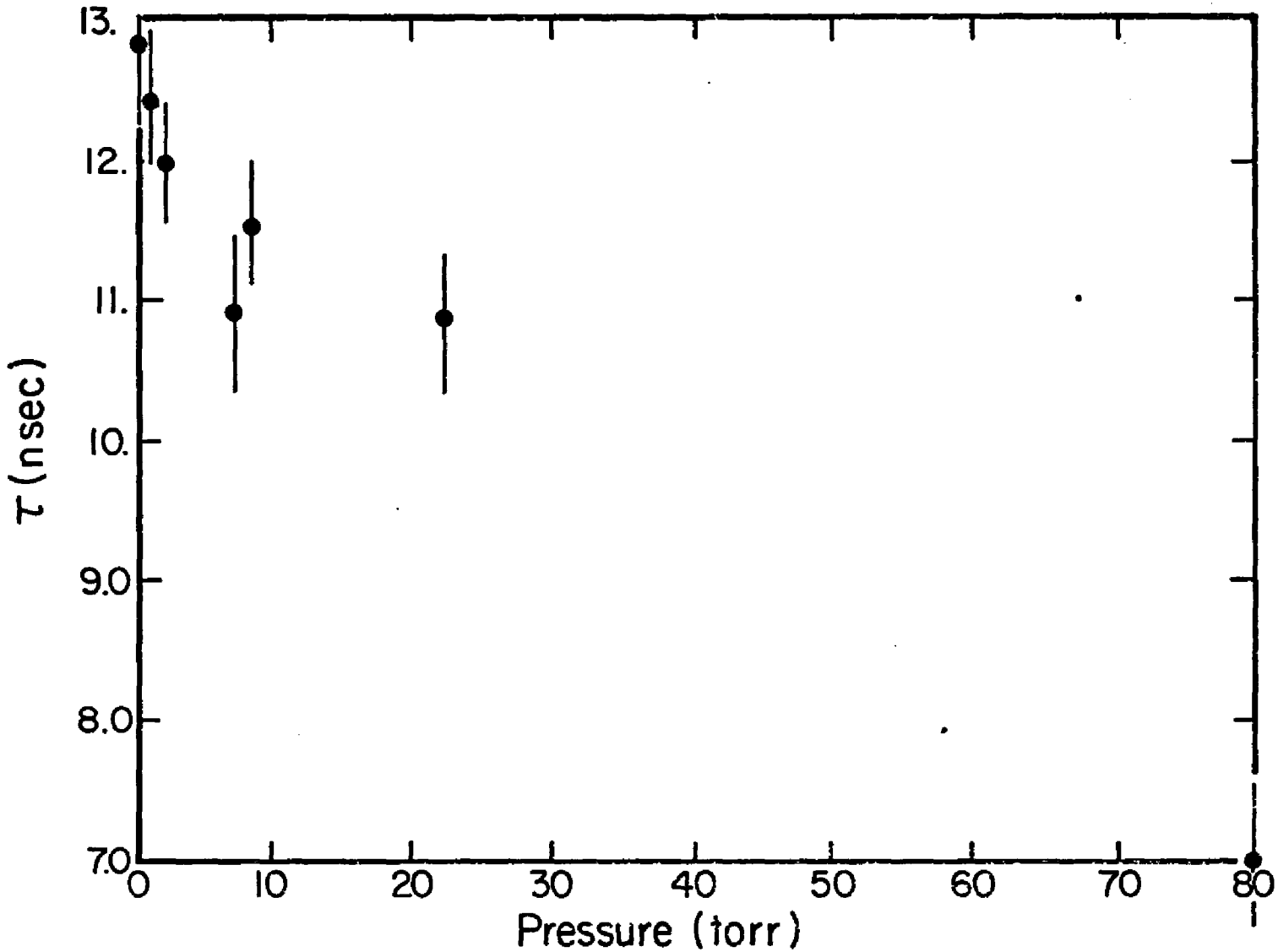
13.
12.
11.
10.
9.0
8.0
7.0
τ (nsec)
0
10
20
30
40
50
60
70
80
Pressure (torr)

TABLE 3

COLLISIONALLY MIXED CA SINGLET LEVELS

STATE	MIXED STATES	$\Delta E (CM^{-1})$
$4p^2\ ^1S_0$	$4p^2\ ^1D_2$	29.4
$4s6s\ ^1S_0$	$4s5d\ ^1D_2^\circ$	107.3
	$4s4f\ ^1F_3^\circ$	664.7
$4s7s\ ^1S_0$	$4s6p\ ^1P_1^\circ$	343.2
$4s8s\ ^1S_0$	$4s6f\ ^1F_3^\circ$	294.9
	$4s7p\ ^1P_1^\circ$	462.1
$4p^2\ ^1D_2$	$4p^2\ ^1S_0$	29.4
$4s5d\ ^1D_2$	$4s5d\ ^3D_3$	171.7

Because observation of the fluorescence signals was usually at the same wavelength as the exciting laser pulse, a large amount of laser light was scattered directly into the PMT. However, the measured lifetimes were unaffected by order-of-magnitude changes in laser intensities, indicating that fluorescence signal distortion due to PMT laser saturation was not a problem. Final data was always taken with fluorescence intensities well below the saturation level of the PMT.

By directly observing the attenuated dye laser pulse shape for the shortest pulses, which were nearly triangular with a width of 4 nsec at the base, the minimum rise time of the PMT-oscilloscope detection system was 1.3 nsec, and the maximum decay time was 1.5 nsec. To see what effect these finite response times would have on the observed lifetimes each triangular laser pulse was assumed to be the response of the PMT-oscilloscope system to a delta function laser signal. This "worst-case" model is presented in Appendix II, where it is seen that the finite system response time has a negligible effect on lifetimes longer than about 7 nsec, and only a slight effect on lifetimes as short as 4.5 nsec. Thus only the Ca $^1P_1$ state lifetime and the Al and Ga $^2S_{1/2}$ state lifetimes would be significantly effected.

For the Ca $^1P_1$ measurements, the maximum possible error due to the system's response time is about 0.2 nsec, while for the Al and Ga $^2S_{1/2}$ state measurements the maximum error is about 0.08 nsec. The effect on all the other lifetime measurements is even less and totally negligible. Thus any error due to the finite system response time is small compared to the estimated error, as quoted in Tables 4 - 6.

4.4 RESULTS AND DISCUSSION (SHORT LIFETIMES)

The results of the measurements of short lifetimes of excited states in the Group II and Group III atoms are presented in Tables 4 - 6, along with values obtained for the lifetimes by other workers. For each of our measured

TABLE 4

LIFETIMES OF THE $^3S_1$ STATES IN MG, CA AND SR

	Level Lifetime (nsec)			
ATOM	THIS EXPT.	OTHER EXPT.	THEORY	REF.
Magnesium	9.7 ± 0.5	13.0 ± 1.0		29
		10.0 ± 2.0		30
		10.1 ± 0.8		31
			9.1	32
			12.8	33
			10.0	34
Calcium	11.7 ± 0.6	15.4 ± 3.1		30
		10.7 ± 1.0		35
		11.7 ± 1.7		36
			16.0	33
			14.5	37
			14.5	38
Strontium	12.9 ± 0.7	9.5 ± 1.9		39
		11.4 ± 2.3		30
		10.9 ± 1.1		40
			19.5	33
			16.0	41
			17.4	37

TABLE 5

LIFETIMES OF VARIOUS STATES IN THE

SINGLET SERIES OF CA

	Level Lifetime (nsec)		
LEVEL	THIS EXPT.	OTHER EXPTS.	REF
$4s4d\,^1D_2$	80.2 ± 9.6		
$4p^2\,^1D_2$	14.9 ± 0.9	15.2 ± 2.3	30
		14.8 ± 1.5	42
		17.0 ± 1.5	42
$4s5d\,^1D_2$	22.2 ± 1.3	25.0 ± 5.0	30
		28.0 ± 2.0	42
		24.0 ± 3.0	42
$4s6d\,^1D_2$	71.6 ± 5.0		
$4p^2\,^1S_0$	88.9 ± 3.0		
$4s6s\,^1S_0$	12.6 ± 0.8		
$4s7s\,^1S_0$	62.4 ± 4.3		
$4s8s\,^1S_0$	118.3 ± 6.3		
$4s4p\,^1P_1$	4.7 ± 0.5		

TABLE 6

LIFETIME OF THE LOWEST $^2S_{\frac{1}{2}}$ STATE OF

AL, GA, IN, AND TL

	Level Lifetime (ns)				
ATOM	THIS EXPT.	OTHER EXPT.	METHOD	THEORY	REF
Aluminum	6.8 ± 0.3		Direct		
		6.94 ± 0.35	Phase-shift		43
		7.05 ± 0.30	Phase-shift		44
		6.2 ± 0.4	Beam foil		45
		6.4 ± 0.4	Beam foil		45
				6.35	46
Gallium	7.0 ± 0.4		Direct		
		6.8 ± 0.3	Level crossing		47
		6.9 ± 0.5	Beam foil		48
		7.6 ± 0.4	Phase-shift		49
				6.34	46
Indium	7.4 ± 0.3		Direct		
		7.0 ± 0.3	Level crossing		47
		7.5 ± 0.3	Phase-shift		49
		8.5 ± 0.1	Phase-shift		50
				6.46	46
Thallium	7.8 ± 0.3		Direct		
		7.65 ± 0.2	Phase-shift		49
		7.45 ± 0.2	Level crossing		47
		7.61 ± 0.16	Level crossing		51
		7.55 ± 0.08	Level crossing		52
				6.98	46

lifetimes, the quoted error is the standard deviation from the average obtained in the final data run.

Histograms of data taken in the final data run for the Tl $^2S_{1/2}$ state and the Mg $^3S_1$ state lifetime measurements are presented in Figure 17-18. The data are seen to fit gaussians quite well, which is typical of the measurements where a large number of data points were taken.

It is seen from Tables 4 and 5 that the lifetimes measured in these experiments are in general agreement with those obtained by other experimenters, but are more precise. For most of the lifetimes measured in the Ca singlet series, (Table 5), no other experimental data exists. The results of the lifetime measurements in the Group III atoms, summarized in Table 6, are in excellent agreement with most existing data. The agreement between the results of these varied experiments indicates that the recent relativistic calculations of Migdadek (1975) are too low.

4.5 SR $^3P_1$ STATE MEASUREMENTS

The flashlamp-pumped dye laser used to populate the $^3P_1$ state was set to the 6893 Å $^3P_1 \leftrightarrow {}^1S_0$ transition by observing the laser output with a ½-meter spectrophotometer. This transition, along with transitions to other excited states in the Sr triplet series, is shown in Figure 10. To obtain a Sr vapor density suitable for observing fluorescence signals the Sr cell was heated to about 550°C, which corresponds to a Sr vapor pressure of about 1.5×10^{-2} Torr. The

FIGURE 17

HISTOGRAM OF THE TL $^2S_{1/2}$ STATE LIFETIME DATA

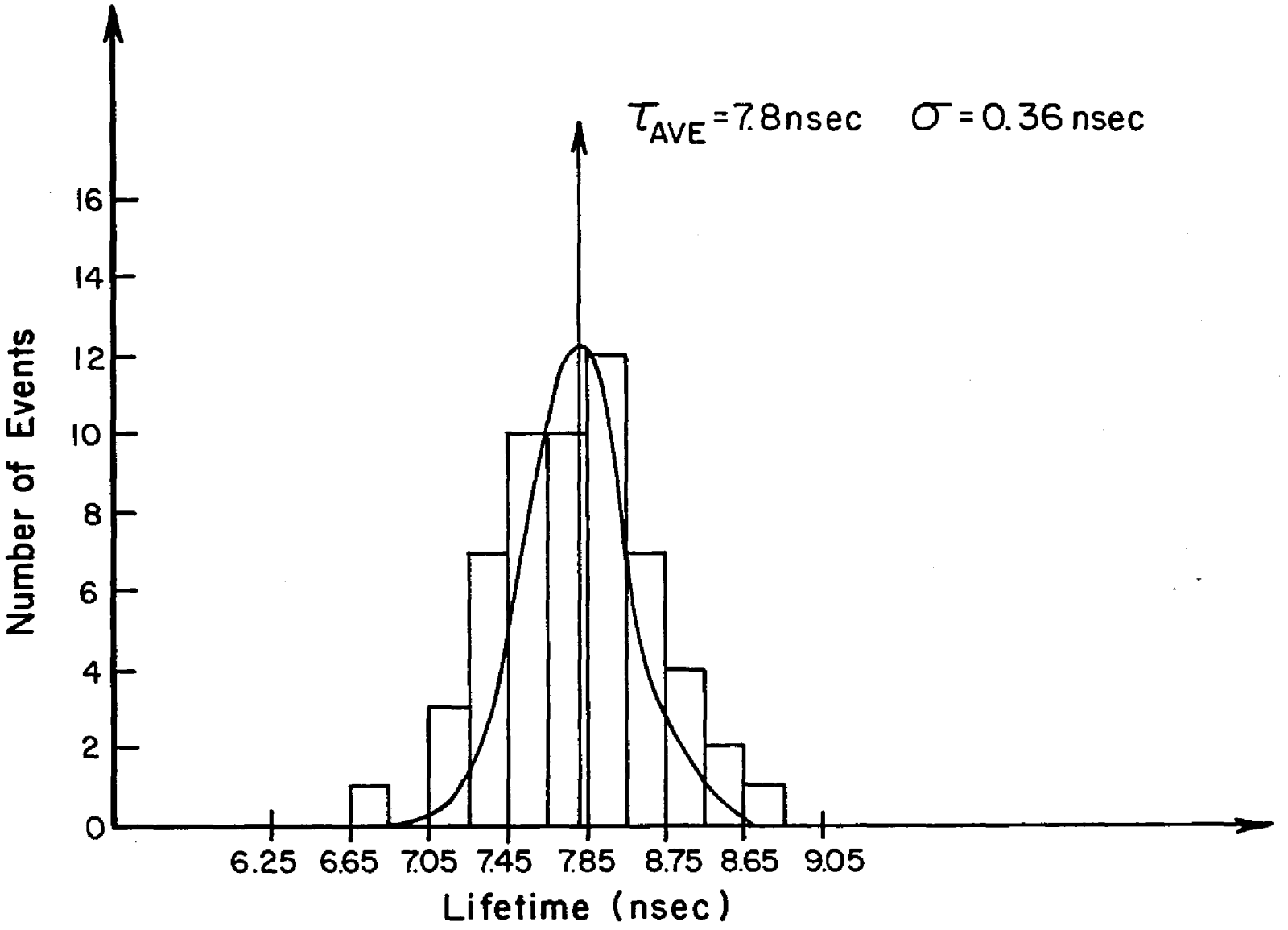
τ_{AVE} = 7.8 nsec
σ = 0.36 nsec
Number of Events
0
2
4
6
8
10
12
14
16
6.25
6.65
7.05
7.45
7.85
8.75
8.65
9.05
Lifetime (nsec)

FIGURE 18

HISTOGRAM OF THE MG $^3S_1$ STATE LIFETIME DATA

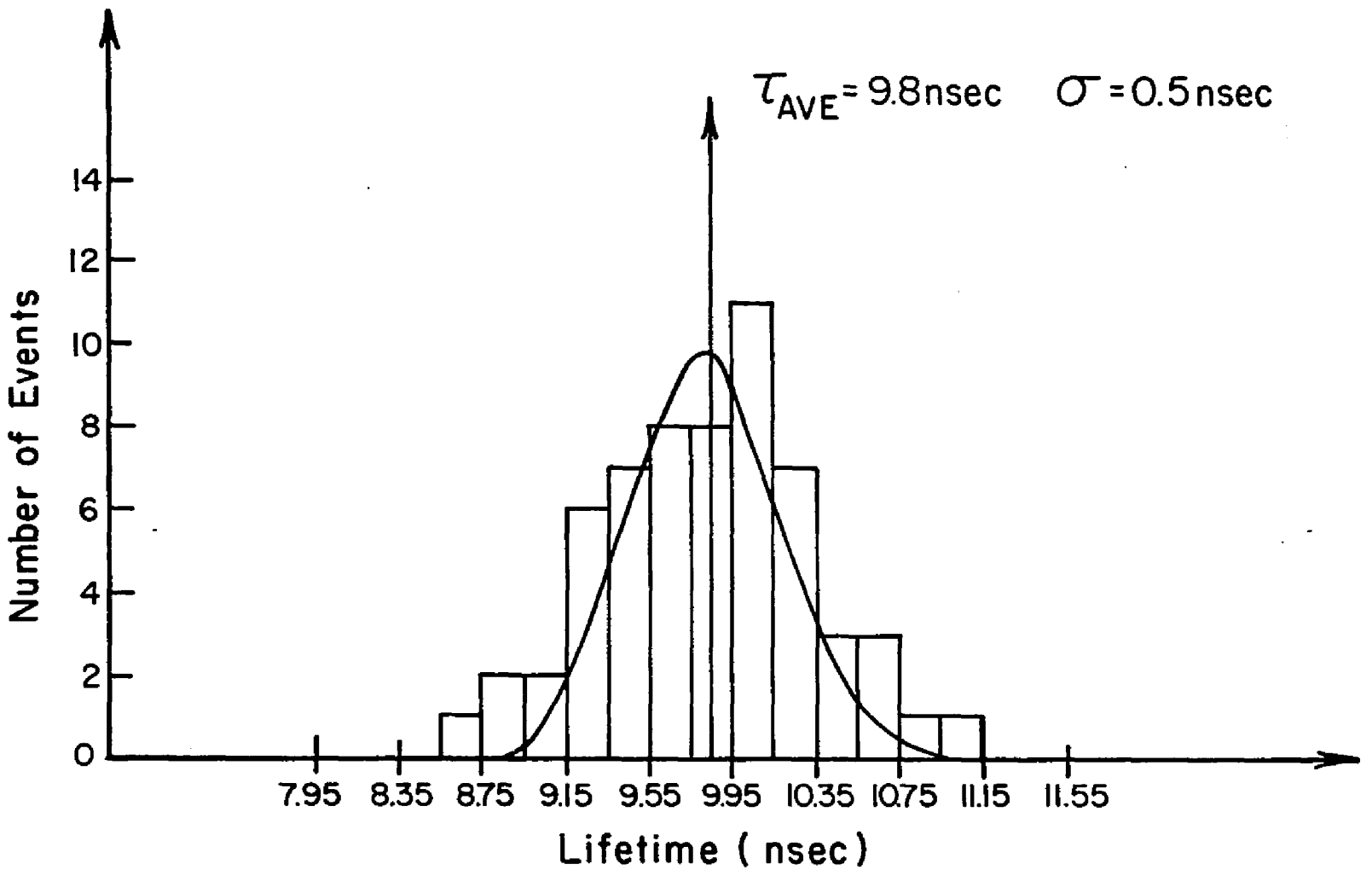
τ_{AVE} = 9.8nsec
σ = 0.5nsec
Number of Events
0
2
4
6
8
10
12
14
7.95
8.35
8.75
9.15
9.55
9.95
10.35
10.75
11.15
11.55
Lifetime (nsec)

fluorescence signals thus obtained were optimized by tuning the laser wavelength until a maximum signal amplitude was obtained. Fluorescence signals were directly observed at right angles to the exciting laser beam by a PMT-interference filter combination. The signals were displayed on the Tektronix storage oscilloscope, which had an input resistance of about 1 kΩ. Data were taken in the range 370 - 520°C, corresponding to a Sr vapor pressure range of 2×10^{-5} to 6.5×10^{-3} Torr.

Lifetime data was acquired directly from the stored oscilloscope trace of the fluorescence signal. A finely lined graticule made possible accurate recordings of the position of a point on the oscilloscope trace. A result for each stored signal was obtained by plotting the signal amplitude semilogarithmically as a function of time out three lifetimes, starting near t = 0. Data transcribed from the trace of a typical fluorescence signal is shown in Figure 19. As scattered laser light on top of the fluorescence signal was only 1 μsec long, it would show only as a spike at t = 0 on this time scale, and so has been omitted from Figure 19. The slope of the straight line semilog plot yielded each trace's lifetime value. About 25 such traces yielded the measured value for the Sr $^3P_1$ state lifetime.

Before the final data run a number of checks for possible systematic effects on the $^3P_1$ state lifetime were made. These checks are discussed in detail in the next section.

FIGURE 19

DATA FROM A SR $^3P_1$ STATE FLUORESCENCE SIGNAL

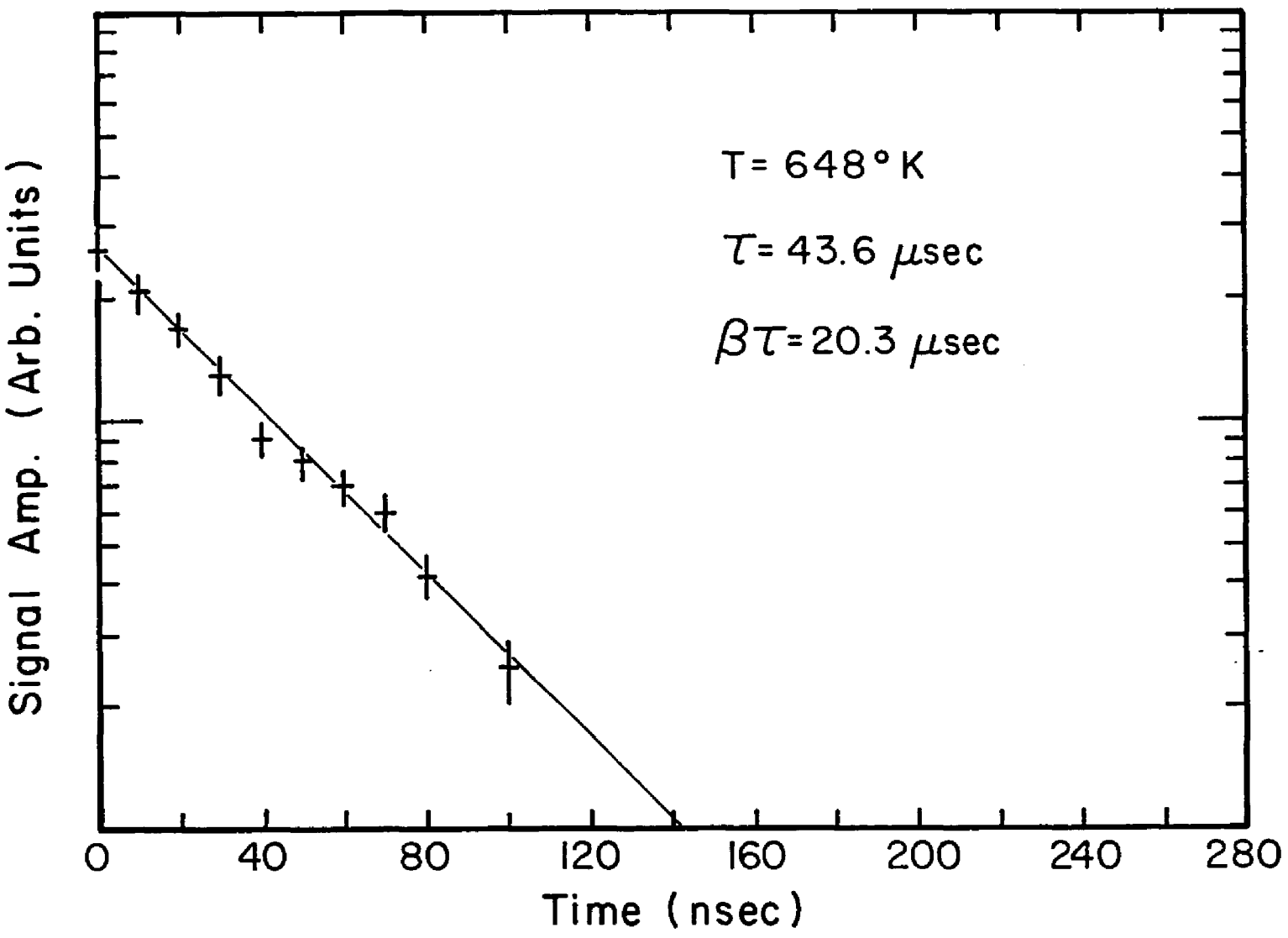
T = 648° K
τ = 43.6 μsec
βτ = 20.3 μsec
Signal Amp. (Arb. Units)
0
40
80
120
160
200
240
280
Time (nsec)

4.6 $^3P_1$ STATE-SYSTEMATIC EFFECTS

The major sources of possible systematic error in the measurements of the $^3P_1$ state lifetime are radiation trapping, quenching of metastable atoms by collisions with impurities or buffer gas atoms, and thermal redistribution, by inert gas atoms, of population among the ^3P fine-structure levels. Photomultiplier saturation by blackbody radiation from the hot oven and by scattered laser radiation are also potential sources of systematic error which must be considered.

Radiation trapping of the 6893 Å fluorescence was eliminated as a source of error by decreasing the Sr vapor pressure until no dependence of the measured lifetime on the Sr vapor density was observed. The vapor pressure was varied from $\sim 3 \times 10^{-5}$ Torr to $\sim 8 \times 10^{-5}$ Torr with no change in the observed lifetime. Increasing the Sr density over an order of magnitude to 7×10^{-4} Torr resulted in only a 7% change in the lifetime. The dependence of the $^3P_1$ state lifetime on the buffer gas pressure and Sr vapor density is shown in Figure 20. As discussed in Chapter II, the lifetime values given have been corrected for mixing to the $^3P_0$ and $^3P_2$ fine structure levels.

To prevent diffusion of Sr vapor to the cell windows, and to inhibit migration of Sr vapor from the interaction region to unlined regions of the cell, an inert buffer gas was used in the $^3P_1$ state lifetime measurements. The gas, as discussed in Chapter II, has the effect of mixing, by

FIGURE 20

SR $^3P_1$ STATE LIFETIME VS. HE PRESSURE

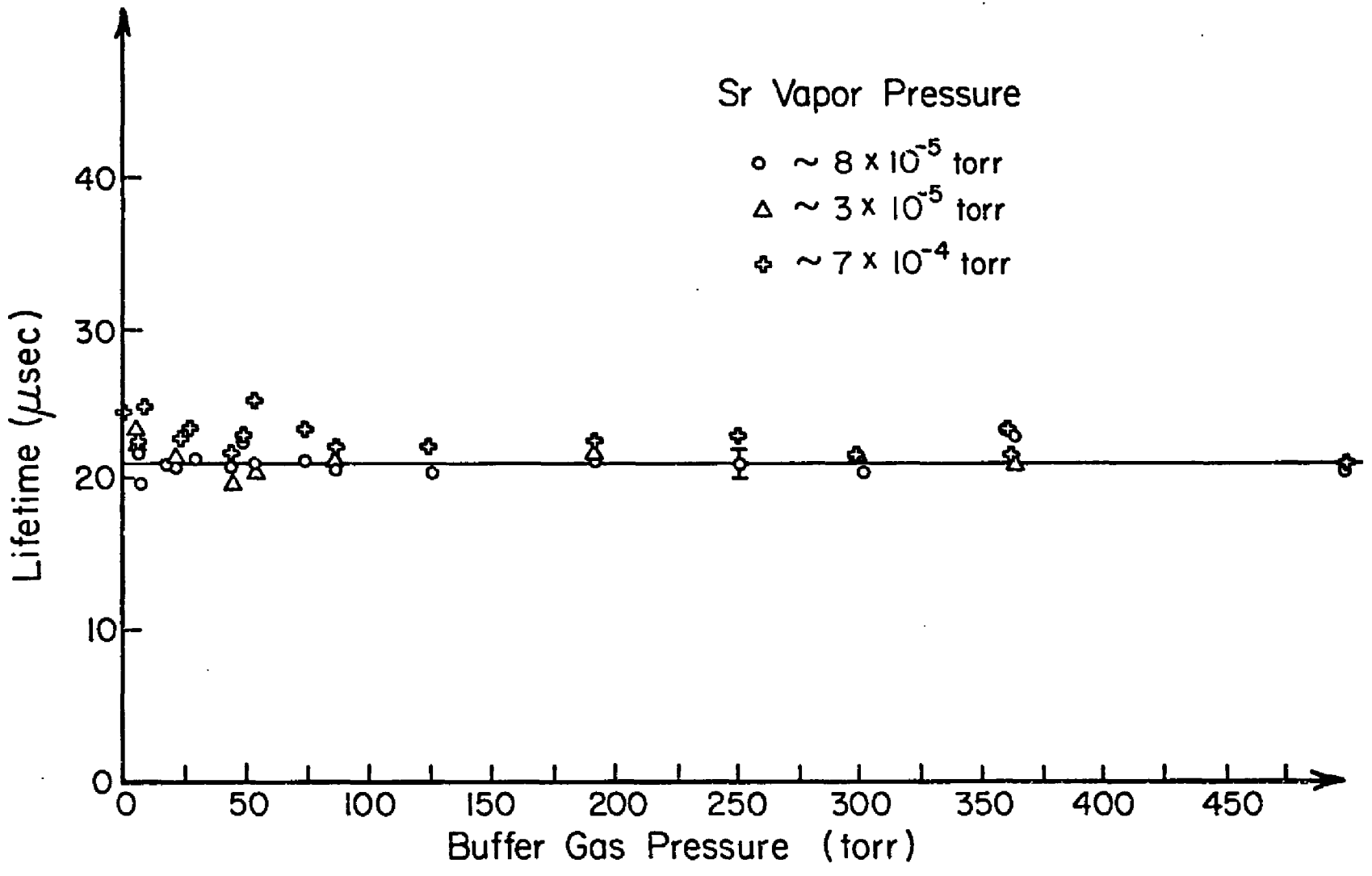
Sr Vapor Pressure
o ~ 8 x 10^-5 torr
Δ ~ 3 x 10^-5 torr
✣ ~ 7 x 10^-4 torr
Lifetime (μsec)
0
10
20
30
40
0
50
100
150
200
250
300
350
400
450
Buffer Gas Pressure (torr)

inelastic collisions, the various fine-structure sublevels of the ^3P multiplet. For the measurements made in He buffer gas, no gas pressure dependence of the observed lifetime (Figure 20) was seen, indicating that the fine-structure levels were in thermal equilibrium. This being the case, the observed decay rate can be converted to the natural decay rate by using appropriate values of $\beta(T)$. For the non-radiation trapped data, $\beta(T)$ ranged from 2.198 to 2.212. Using these values for $\beta(T)$, the $^3P_1$ state lifetime value was determined to be 21.0 ± 1.0 μsec.

For inert gases other than He, a strong gas pressure dependence of the observed lifetime was found, which was attributed to non-thermalized populations in the $^3P_2$, $^3P_1$ and $^3P_0$ levels. This was borne out by absorption monitoring of the population of the ^3P fine-structure levels as a function of inert gas pressure. It was found that, upon excitation of the $^3P_1$ level with the laser, the $^3P_0$ and $^3P_2$ level populations increased to some maximum in a time on the order of the natural decay time of the $^3P_1$ state. This rise time must be very fast compared to the natural decay time if thermal equilibrium is to be established among the various levels. With the addition of small amounts of He gas to the other gas already in the cell, the rise time was seen to go to a very short value, establishing that the He gas does indeed thermalize the levels. The absorption monitoring technique used in these diagnostic measurements is described in detail by Wright et al.[28].

The pressure dependence of the observed fluorescence lifetime was studied in Kr and Xe inert gases. Insofar as the data taken in these measurements illustrates how strongly the observed lifetime is affected when there is a pressure dependence, some of it will be included here. In general, what was observed was a doubly exponential fluorescence decay whose decay rates depended on the inert gas pressure and on the inert gas. For high gas pressures, the doubly exponential signal became a single exponential one with a decay time equal to the He gas thermal equilibrium value (at that temperature). For low gas pressures, the signal was clearly a double exponential, and both decay rates depended linearly on the gas pressure. These effects are illustrated in Figures 21 and 22. The dependence of the smaller rate on temperature in Kr gas is shown in Figure 23.

These data can be understood in a general way by approximating the three level ^3P multiplet by a two level system and solving the rate equations for this case. This model is presented in Appendix III, where it is seen that a linear gas pressure dependence of the two rates is expected at low pressures. The temperature dependence in this model arises from an increase in impurity quenching at zero buffer gas pressure and from the increase of the relative velocities of the colliding partners as the cell temperature is increased. Unfortunately, as the ^3P multiplet is really a three level system with three independent mixing rates, no absolute values for the mixing rates can be derived from this data. The data

FIGURE 21

SR $^3P_1$ STATE SHORT DECAY TIME

VS. KR GAS PRESSURE

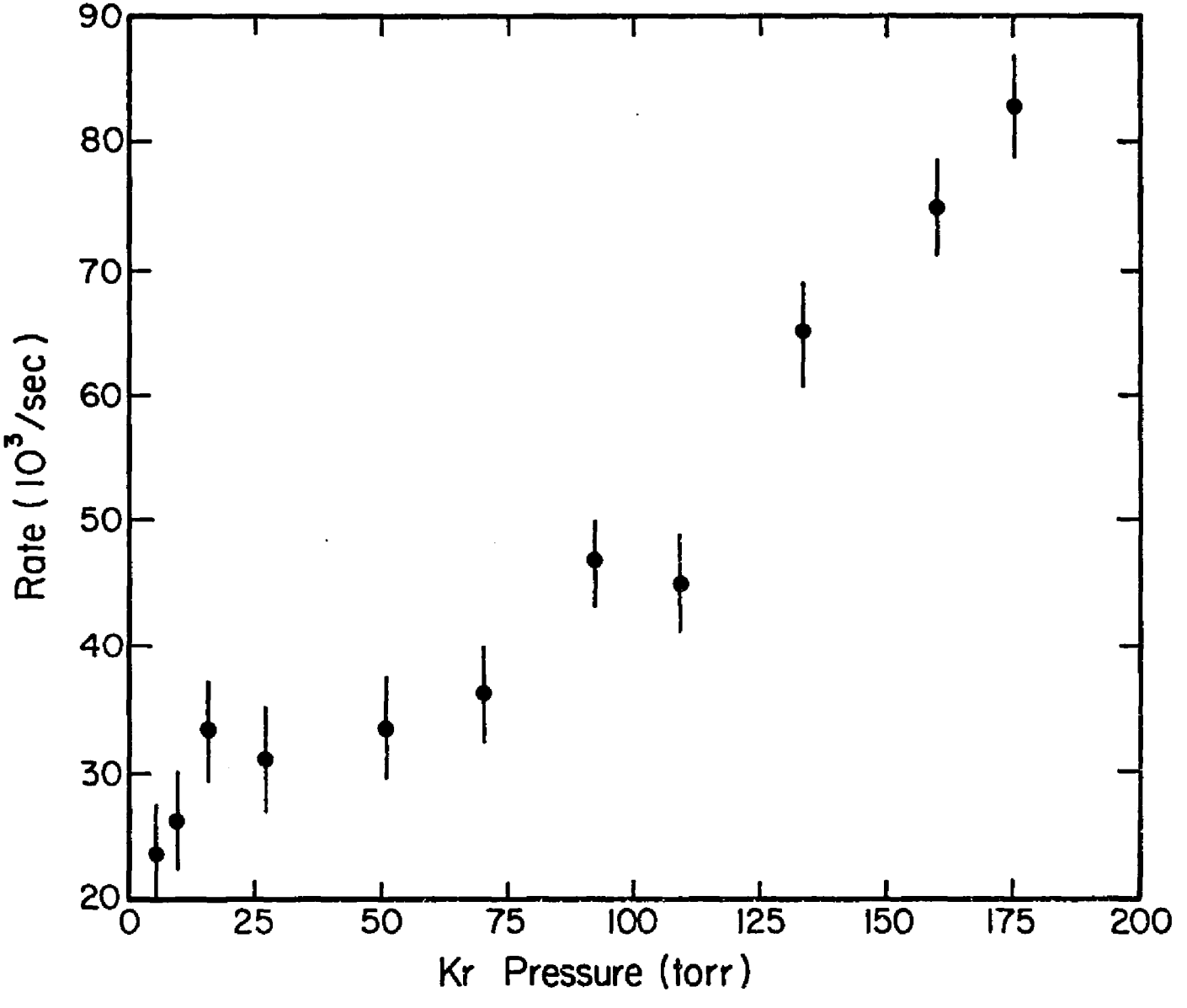
90
80
70
60
50
40
30
20
Rate (10^3/sec)
0
25
50
75
100
125
150
175
200
Kr Pressure (torr)

FIGURE 22

SR $^3P_1$ STATE LONG DECAY TIME VS.

KR AND XE GAS PRESSURE

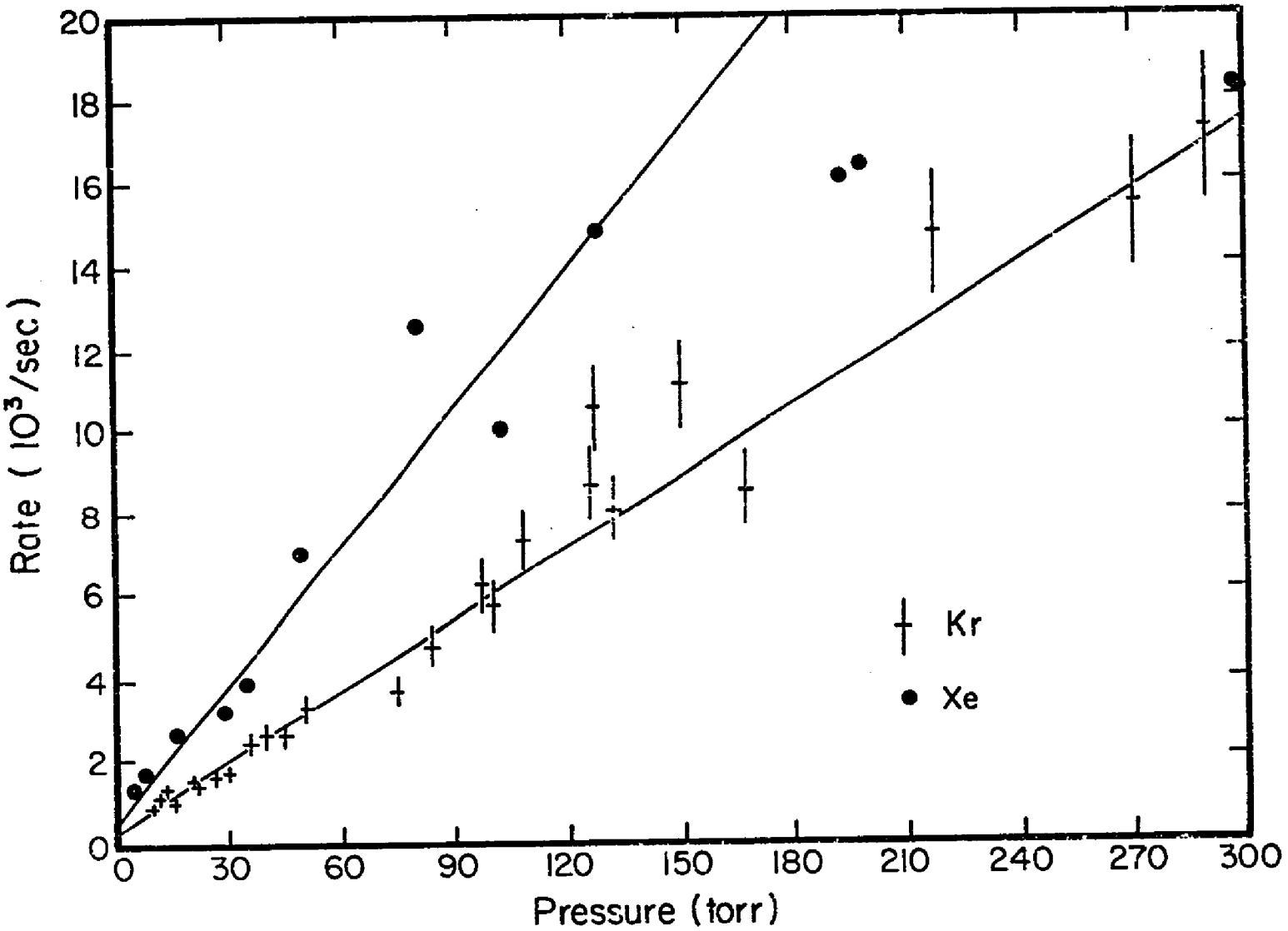
20
18
16
14
12
10
8
6
4
2
0
Rate (10^3/sec)
0
30
60
90
120
150
180
210
240
270
300
Pressure (torr)
Kr
Xe

FIGURE 23

SR $^3P_1$ STATE LONG DECAY TIME

VS. TEMPERATURE

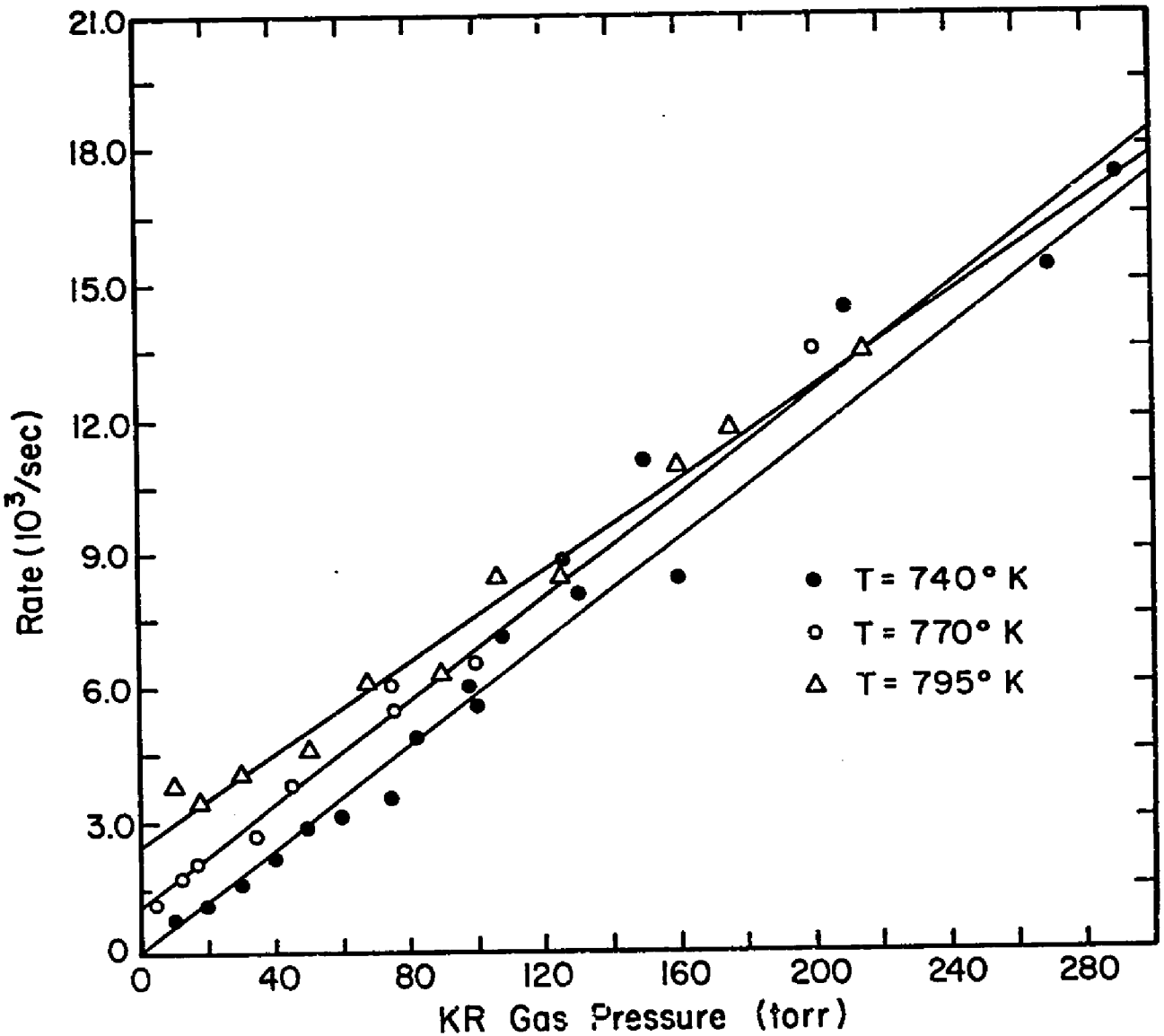
21.0
18.0
15.0
12.0
9.0
6.0
3.0
0
Rate (10^3/sec)
0
40
80
120
160
200
240
280
KR Gas Pressure (torr)
T = 740° K
T = 770° K
T = 795° K

thus serves principally to illustrate that the observation of no pressure dependence on He gas pressure is further evidence that the Sr fine structure levels were in thermal equilibrium for the measurements in that gas.

To eliminate possible saturation of the PMT by glow from the hot oven or from stray light, the fluorescence signals were viewed through a 50Å bandwidth interference filter centered at 6900Å. Attenuation of the fluorescence signals with neutral density filters resulted in no change in the measured lifetime, eliminating PMT saturation by the fluorescence signals as a source of error in the experiment. No change in the observed lifetime was found when attenuating the laser with neutral density filters, eliminating stimulated emission and PMT saturation by laser light as sources of systematic error.

4.7 RESULTS ($^3P_1$ STATE)

The value obtained for the $^3P_1$ state lifetime, along with a summary of the most recent experimental and theoretical values obtained by other workers for this lifetime, is presented in Table 7. The result for the $^3P_1$ lifetime of 21.0 ± 1.0 μsec is in excellent agreement with the theoretical prediction of Luc-Koenig and the experimental value of Ma et al.

TABLE 7

SUMMARY OF RECENT THEORETICAL AND EXPERIMENTAL VALUES FOR THE SR $^3P_1$ LIFETIME

METHOD	LIFETIME (μsec)	REF
Hook method	25	53
Emission Spectrum	16.4 (3)	54
Atomic Beam	74 (28)	55
Double Resonance	21 (3)	56
Double Resonance	6.4 (6)	57
Theory	19.9	58
Theory	14.5	59
Laser Excitation	21 (1)	This Expt.

The value of 21.0 μsec obtained in this experiment is a straight average of the non-radiation trapped data presented in Figure 11. A linear least squares fit to this data yielded a zero pressure intercept of 21.0 μsec. The quoted error represents the standard deviation from the arithmetic average of the He buffer gas, low temperature data.

4.8 CONCLUSIONS

Lifetimes of a large number of states in the Group II and Group III atoms have been directly measured. These lifetimes are summarized in Tables 4-7. For a number of these states no experimental lifetime data existed prior to these

measurements.Where other experimental data is available, general agreement is found among the results of the direct measurements and the results of the other experiments. However, the directly measured lifetimes are more precise and, as our quoted error represents an upper limit to possible systematic errors, probably more accurate.

REFERENCES

Chapter I.

[1]S.L. Goldberg, E.A. Müller, L.H. Aller, Astroph. J. Supplement, V.5, (1960.

[2]J. Marek, N. Kiemax, J. Phys. B9, No. 16, L483 (1976).

[3]H. Lundberg and S. Svanberg, Phys. Lett. A56, No. 1, 31 (1976).

[4]T.F. Gallagher, S.A. Edelstein, and R.M. Hill, Phys. Rev All, No. 5, 1504 (1975).

[5]K. Siomos, H. Figger, H. Walther, Z. Physik A272, 355 (1975).

[6]H.A. Bethe, E.E. Salpeter, Quantum Mechanics of One- and Two-Electron Atoms (Springer-Verlag, 1957) p 248-250.

[7]H.A. Bethe, R. Jackiw, Intermediate Quantum Mechanics, (Benjamin, 1968) 3rd ed., Chap. 11, p. 224.

[8]M. Mizushima, Quantum Mechanics of Atomic Spectra and Atomic Structure (Benjamin, New York, 1970), Chap. 7, p. 216.

[9]C. Laughlin and G.A. Victor, Astrop. Journal 192, 551 (1974).

[10]H. Nussbaumer, Astron & Astrophys. 16, 77 (1972).

[11]E. Luc-Koenig, J. Phys. B7, No. 9, 1052 (1974).

[12]Data from W.L. Weise, M.W. Smith, and B.M. Glennon, NSRDS-NBS4, Atomic Transition Probabilities, V. 1-2 (1966).

[13]M. Mizushima, Quantum Mechanics of Atomic Spectra and Atomic Structure (W.A. Benjamin, New York, 1970), Chapt. 4 p. 89.

Chapter III.

[14]Data from Laser Dyes (technical data), available from New England Nuclear, Watertown, Massachusetts.

[15]Laser Dyes data sheet available from Phase-R Corp., New Durham, New Hampshire.

[16]Private communication - Walter Johnson (RCA Engineer), Needham, Massachusetts.

[17]Purchased from Infrared Industries, Waltham, Mass.

[18]Purchased through Hovey's Camera, Portsmouth, New Hampshire.

[19]Constructed by Anderson Glass Co., Fitzwilliam, New Hampshire.

[20]Purchased from Norton, Co., Newton, Massachusetts.

[21]Purchased from Ventron Corp., Danvers, Massachusetts.

[22]Purchased from Cryogenics East, Billerica, Mass.

Chapter IV.

[23]M. Gross, C. Fabre, P. Pillet, and S. Haroshe, Phys. Rev. Lett. 36, 17, 1035 (1976).

[24]R.H. Dicke, Phys. Rev. 93, 1 99 (1954).

[25]R. Bonifacio and L.A. Logiato, Phys. Rev. A11, 5, 1507 (1975).

[26]N. Skribanowitz, I.P. Herman, J.C. MacGillivray, and M.S. Feld, Phys. Rev. Lett. 30, 8, 309 (1973).

[27]N.P. Penkin, L.N. Shabanova, Optics Spectrosc. 26, 191 (1969).

[28]J.J. Wright, J.F. Dawson, and L.C. Balling, Phys. Rev. A9, 1, 83 (1974).

[29]H.G. Berry, J. Bromander, and R. Buchta, Physica Scripta, V.1, 181 (1970).

[30]H. Kostlin, Z. Physik 178, 200 (1964).

[31]T. Andersen. L. Mølhave, and G. Sørensen, Astrop. Journal 178, 577 (1972).

[32]G.A. Victor and R.F. Stewart, Astroph. Journal Supp. Ser., 31, 237 (1976).

[33]B. Warner, Mon. Not. R. Astron. Soc. 139, 103 (1968).

[34]C. Fischer, Can. J. Phys. 53, 338 (1975).

[35]W. Gornik, D. Kaiser, W. Lange, J. Luther, K. Meier, H.H. Radloff, and H.H. Schulz, Phys. Lett. 45A, 3 219 (1973).

[36]G. Smith and J.A. O'Neill, Astron. and Astrophys. 38, 1 (1975).

[37]P.F. Gruzdev, Optics and Spectroscopy 22, 2, 89 (1967).

[38]E.M. Andersen, V.A. Zilitis, and E.S. Sorokina, Optics and Spectroscopy 23, 4, 279 (1967).

[39]A. Eberhagen, Z. Physik 143, 392 (1955).

[40]U. Brinkmann, Z. Physik 228, 440 (1969).

[41]V.A. Zilitis, Optics and Spectroscopy 24, 5, 438 (1970).

[42]M. Chenevier, J. Dufayard, and J.C. Pebay-Peyroula, Phys. Lett. 25A, 3, 283 (1967).

[43]J. Marek and J. Richter, Astron. and Astrophys. 26, 155 (1973).

[44]P.T. Cunningham, J. Opt. Soc. Am. 58, 11, 1507 (1968).

[45]T. Andersen, K.A. Jessen, and G. Sørensen, J. Opt. Soc. Am. 59, 9, 1197 (1969).

[46]J. Migdałek, Can. J. Phys. 54, 118 (1975).

[47]M. Norton and A. Gallagher, Phys. Rev. A3, 915 (1971).

[48]T. Andersen and G. Sørensen, Phys. Rev. A., 5, 2447 (1972).

[49]P. Cunningham and J.K. Link, J. Opt. Soc. Am. 57, 1000 (1967).

[50]E. Hulpke, E. Paul, and W. Paul, Z. Physik 177, 257 (1964).

[51]M.A. Rebolledo and E. Bernabeu, Rev. Acad. Cienc. Zargoza 28, No. 4, 467 (1973).

[52]J.C. Hsieh and J.C. Baird, Phys. Rev A6, 141 (1972).

[53]N.P. Penkin, J. Quant. Spectrosc. Radiat. Transf. 4, 41 (1964).

[54]A. Eberhagen, Z. Physik 143, 392 (1955).

[55]F. Ackermann, M. Baumann and J. Gayler, Z. Naturforsh A21, 664 (1966).

[56]I.J. Ma, G. ZuPutlitz, G. Schutte, Z. Physik 208, 266 (1968).

[57]M. Baumann, M. Holder, H. Vogele, Phys. Verhandl DPG4, 41 (1964).

[58]E. Luc-Koenig, J. Phys. B7, 1052 (1974).

[59]B. Warner, Mon. Not. R. Astron. Soc. 140, 53 (1968).

BIBLIOGRAPHY

Bethe, H.A. and R. Jackiw. Intermediate Quantum Mechanics .(W.A. Benjamin, Inc., Reading, Mass. 1968).

Bethe, H.A. and E.E. Salpeter. Quantum Mechanics of One-and Two-Electron Atoms.(Springer-Verlag, Berlin, 1957).

Mizushima, M. Quantum Mechanics of Atomic Spectra and Atomic Structure.(W.A. Benjamin, Inc., New York, 1970).

Weise, W.L., M.W. Smith, and B.M. Glennon. Atomic Transition Probabilities (NSRDS-NBS4) (U.S. Government Printing Office, Washington, D.C., 1966).

APPENDIX I

The rate equations for a two level system with mixing are given by

$$\frac{dN_1}{dt} = -(\Gamma_1 + \gamma_{12})N_1 + \gamma_{21}N_2$$

$$\frac{dN_2}{dt} = -(\Gamma_2 + \gamma_{21})N_2 + \gamma_{12}N_1 .$$

The rates in these equations are defined in Figure 24a. Γ_1 and Γ_2 are natural decay rates and γ_{12} and γ_{21} are mixing rates which depend linearly on the pressure of the inert mixing gas. Level 1 has degeneracy g_1 and level 2 has degeneracy g_2.

If level 1 is populated by a short laser pulse at t = 0, then the initial conditions are

$$N_1(0) = N_o$$

$$N_2(0) = 0$$

With these conditions, the solution to the rate equations for $N_1(t)$ is given by

$$N_1(t) = \frac{N_o}{\beta - \alpha}\left[(\beta - \Gamma_1 - \gamma_{12})e^{-\alpha t} + (\Gamma_1 + \gamma_{12} - \alpha)e^{-\beta t}\right],$$

FIGURE 24

RATES FOR MIXING IN (a.) NEARBY CA

LEVELS AND (b.) SR ^{3}P LEVELS

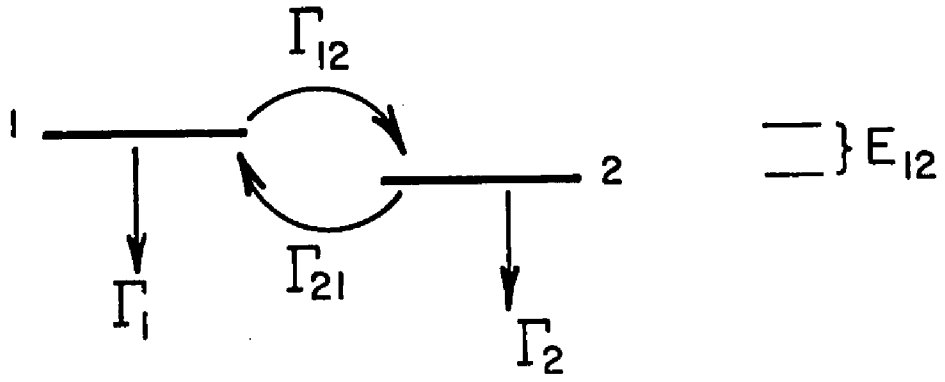
Γ_{12}
1
2
E_{12}
Γ_{21}
Γ_1
Γ_2

(a)

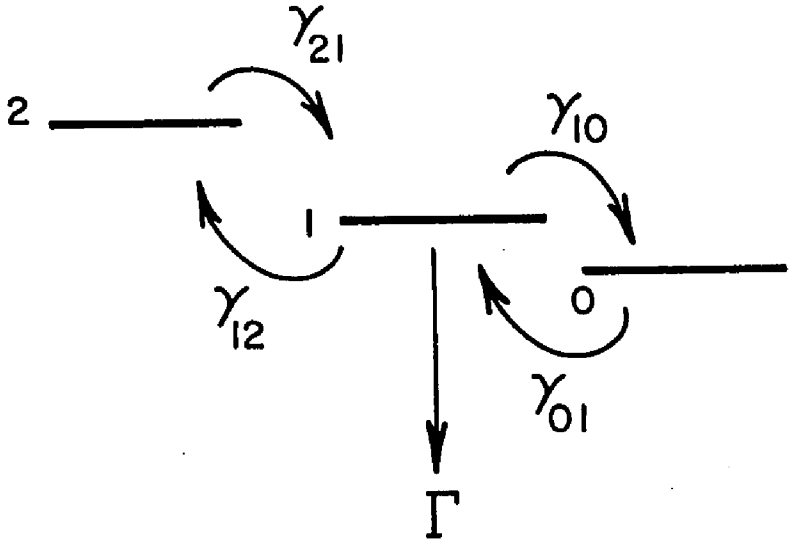
γ_{21}
2
γ_{10}
1
γ_{12}
0
γ_{01}
Γ

(b)

where

$$\begin{Bmatrix} \alpha \\ \beta \end{Bmatrix} = \frac{\Gamma_1 + \Gamma_2 + \gamma_{12} + \gamma_{21}}{2} \left[1 \begin{Bmatrix} + \\ - \end{Bmatrix} \sqrt{1 - \frac{4\left[(\Gamma_1+\gamma_{12})(\Gamma_2+\gamma_{21}) - \gamma_{12}\gamma_{21}\right]}{(\Gamma_1 + \Gamma_2 + \gamma_{12} + \gamma_{21})^2}} \right].$$

In the usual case, $\Gamma_1 \simeq \Gamma_2$ and $\Gamma_1 , \Gamma_2 >> \gamma_{12} , \gamma_{21}$. Thus, if we set $\Gamma_1 = \Gamma_2 = \Gamma/2$, then α and β become

$$\begin{Bmatrix} \alpha \\ \beta \end{Bmatrix} = \begin{Bmatrix} \gamma_{12} + \gamma_{21} + \Gamma/2 \\ \Gamma/2 \end{Bmatrix}.$$

From detailed balancing the ratio of the mixing rates is given by

$$\frac{\gamma_{21}}{\gamma_{12}} = \frac{g_1}{g_2} e^{-E_{12}/KT} .$$

If mixing is to a highly degenerate final state, then $g_2 >> g_1$ and $N_1(t)$ further reduces to

$$N_1(t) = N_0 e^{-\left(\frac{\Gamma}{2} + \gamma_{12} + \gamma_{21}\right)t} .$$

As the mixing rates increase linearly in the pressure of the mixing gas, the observed decay rate $\Gamma/2 + \gamma_{12} + \gamma_{21}$ will also increase linearly in gas pressure. This behavior of the rate was observed in the example discussed in Chapter IV.

APPENDIX II

The following is a calculation of the effect of the finite response time of the detection electronics on the observed fluorescence decay time of the excited atoms.

If the response function of a system is $k(t - t')$ and the input to the system $N(t)$, then the Convolution Theorem states that the output signal will be

$$S(t) = \int_{-\infty}^{t} K(t-t')\, N(t')\, dt' .$$

For the case at hand, $N(t)$ is given approximately by equations (7) in Chapter II.

To obtain an estimate for $k(t - t')$, it was assumed that our shortest observed laser pulses were generated by a delta function input signal. This is a "worst case" calculation, in that the laser pulses certainly had some finite width. The shortest laser pulses were approximately triangular, and could be well represented by

$$S(t) = S_0 \left[e^{-t/\tau_1} - e^{-t/\tau_2} \right] , \quad (\tau_1 > \tau_2) .$$

Here S_0 is a constant and τ_1 and τ_2 have the values 1.5 and 1.2, respectively. All time variables have units of nsec. If $S(t)$ is the response to an input $N(t)$, then $K(t-t')$ is given by

$$K(t-t') = e^{-(t-t')/\tau_1} - e^{-(t-t')/\tau_2} ,$$

where we have put, for convenience, $S_o = 1$.

Typical laser pulses used to populate excited states has widths of about 10 nsec at the base, which means that we want the solutions S(t) for t > 10 nsec. Using N(t) from Chapter II, S(t) is given by

$$S(t) = A e^{-t/1.2} + B e^{-t/1.5} + C e^{-\Gamma t} ,$$

where the constants A, B, and C are

$$A = -\left[4840 + 5807\Gamma + \frac{1}{1/1.2 - \Gamma}\left\{ 64 + (C_1 + C_2) e^{+10\left(\frac{1}{1.2} - \Gamma\right)} - C_1 e^{+5\left(\frac{1}{1.2} - \Gamma\right)} \right\} \right],$$

$$B = 1096 - 2107\Gamma + \frac{1}{1/1.5 - \Gamma}\left\{ 27 + (C_1 + C_2) e^{+10\left(\frac{1}{1.5} - \Gamma\right)} - C_1 e^{+5\left(\frac{1}{1.5} - \Gamma\right)} \right\},$$

$$C = C_2 \left\{ \frac{1}{1/1.5 - \Gamma} - \frac{1}{1/1.2 - \Gamma} \right\}.$$

The quantities C_1 and C_2 are given by

$$C_1 = 1 - 2e^{5\Gamma}$$

$$C_2 = 1 - 2e^{5\Gamma} + e^{10\Gamma} .$$

In the expression for S(t), the important thing is the amplitude of the first two terms compared to that of the last term. If the contribution to S(t) from these terms is negligible, then the system response time will have a negligible effect on the observed lifetime. The approximate time (t_o) at which these terms contribute 4% to the total signal amplitude is listed in Table 8 for several values of Γ. Also included are values for the coefficients A, B, and C occuring in S(t). The value 4% is chosen because it is well below the error in estimating the amplitude of the fluorescence decay curve at any time. It should be noted that for times much longer than t_o, the contribution to the amplitude of the fluorescence decay curve from the A and B terms in S(t) it totally negligible

TABLE 8

COEFFICIENTS OF THE CALCULATED SIGNAL, S(t)

τ (nsec)	Γ (1/nsec)	100A	100B	100C	t_o (nsec)
4.5	0.222	392.4	-116.4	2.55	15
5.0	0.200	308.4	-102.3	1.66	15
6.8	0.147	117.0	- 45.3	0.55	14
7.8	0.128	87.2	- 34.2	0.36	13

APPENDIX III

If the buffer gas pressure is sufficiently low, or the inelastic collision cross-section small, then the buffer gas-Sr atom collisions will not thermalize the ^3P levels, and the mixing rates among the various levels must be taken into account. The rate equations for a three level system can be written as

$$\frac{dN_2}{dt} = -\gamma_{21} N_2 + \gamma_{12} N_1 \quad ,$$

$$\frac{dN_1}{dt} = -(\Gamma + \gamma_{12} + \gamma_{10}) N_1 + \gamma_{21} N_2 + \gamma_{01} N_1 \quad ,$$

$$\frac{dN_0}{dt} = -\gamma_{01} N_0 + \gamma_{10} N_1 \quad .$$

The rates in these equations are defined in Figure 24b. Note that mixing between the well separated (in energy) $^3P_2$ and $^3P_0$ levels has been neglected. Assuming that N_2 and N_0 are equal requires that we set $\gamma_{21} = \gamma_{01}$ and $\gamma_{12} = \gamma_{10}$, in order that the rate equations be self consistent. With $N_2 = N_0 = N$, the equations become

$$\frac{dN}{dt} = -\gamma_{21} N + \gamma_{12} N_1 \quad ,$$

$$\frac{dN_1}{dt} = -(\Gamma + 2\gamma_{12}) N_1 + 2\gamma_{21} N \quad .$$

The solution to these coupled equations is straight forward, and for $N_1(t)$ is given by

$$N_1(t) = \frac{N_1(0)}{\alpha - \beta}\left[(\Gamma + 2\gamma_{12} - \beta)e^{-\alpha t} + (\Gamma + 2\gamma_{12} - \alpha)e^{-\beta t}\right].$$

$N_1(0)$ is the initial population in the ^3P level and the rates α and β are given by

$$\left\{ \begin{matrix} \alpha \\ \beta \end{matrix} \right\} = \left\{ \frac{\Gamma + 2\gamma_{12} + \gamma_{21}}{2}\left[1 \pm \sqrt{1 - \frac{4\Gamma\gamma_{21}}{(\Gamma + 2\gamma_{12} + \gamma_{21})^2}}\right] \right\}.$$

For two body collisions the mixing rate γ_{12} is given by

$$\gamma_{12} = N\sigma_{12}\bar{v} = \frac{g_2}{g_1} e^{-E_{21}/kT} \gamma_{21} ,$$

where detailed balancing has been used to obtain the last expression. In these expressions, $\bar{v}$ is the magnitude of the relative velocity of the collision partners and σ_{12} (σ_{21}) is the mixing cross-section for the two levels.

Expanding α and β to the first order in the mixing rates yields for $N_1(t)$

$$N_1(t) = \frac{N_1(0)}{\Gamma - (2\gamma_{12} - \gamma_{21})}\left[\Gamma e^{-(\Gamma + 2\gamma_{12})t} - (2\gamma_{12} - \gamma_{21})e^{-\gamma_{21}t}\right].$$

It is clear from this expression for $N_1(t)$ that this model predicts the observed signals (double exponential) and the linear gas pressure dependence of the observed decay rates. The increase in the $P = 0$ intercept with increasing temperature for the long lifetime data (Figure 23) can be understood

by including metastable quenching in this model. The ratio γ_{12}/γ_{21} is approximately 2 for the Kr data at T = 790°K, in rough agreement with this ratio calculated from detailed balancing (about 3).

Unfortunately, as the ^3P multiplet is a three level system, the model presented here cannot be used to obtain absolute mixing cross-sections for the $^3P_{2,1,0}$ levels. However, the model is of value in that it describes the qualitative features of the data and strengths and argument that the mixing in He buffer gas was complete.